J|A|C|S ARTICLES

Published on Web 06/24/2010

Development Plus Kinetic and Mechanistic Studies of a Prototype Supported-Nanoparticle Heterogeneous Catalyst Formation System in Contact with Solution: Ir(1,5-COD)Cl/γ-Al_2O_3 and Its Reduction by H_2 to $Ir(0)_n/\gamma$-Al_2O_3

Joseph E. Mondloch,[†] Qi Wang,[‡] Anatoly I. Frenkel,[‡] and Richard G. Finke*,[†]

Department of Chemistry, Colorado State University, Fort Collins, Colorado 80523, and Department of Physics, Yeshiva University, New York, New York 10016

Received April 9, 2010; E-mail: rfinke@lamar.colostate.edu

Abstract: An important question and hence goal in catalysis is how best to transfer the synthetic and mechanistic insights gained from the modern revolution in nanoparticle synthesis, characterization, and catalysis to prepare the next generation of improved, supported-nanoparticle heterogeneous catalysts. It is precisely this question and to-date somewhat elusive goal which are addressed by the present work. More specifically, the global hypothesis investigated herein is that the use of speciation-controlled, well-characterized, solid oxide supported-organometallic precatalysts *in contact with solution* will lead to the next generation of better *composition,* size- and shape-controlled, as well as highly active and reproducible, supported-nanoparticle heterogeneous catalysts—ones that can also be understood kinetically and mechanistically. Developed herein are eight criteria defining a prototype system for supported-nanoparticle heterogeneous catalyst formation in contact with solution. The initial prototype system explored is the precatalyst, Ir(1,5-COD)Cl/γ-Al_2O_3 (characterized via ICP, CO adsorption, IR, and XAFS spectroscopies), and the well-defined product, $Ir(0)_n/\gamma$-Al_2O_3 (characterized by reaction stoichiometry, TEM, and XAFS). The $Ir(0)_n/\gamma$-Al_2O_3 system proved to be a highly active and long-lived catalyst in the simple test reaction of cyclohexene hydrogenation and in comparison to two literature $Ir(0)_n/Al_2O_3$ heterogeneous catalysts examined under identical conditions. High activity (2.2−4.8-fold higher than that of the literature $Ir(0)_n/Al_2O_3$ catalysts tested under the same conditions) and good lifetime ($\geq$220 000 total turnovers of cyclohexene hydrogenation) are observed, in part by design since only acetone solvent, cyclohexene, and H_2 are possible ligands in the resultant "weakly ligated/labile-ligand" supported nanoclusters. Significantly, the Ir(1,5-COD)Cl/γ-Al_2O_3 + H_2 → $Ir(0)_n/\gamma$-Al_2O_3 heterogeneous catalyst formation kinetics were also successfully monitored using the cyclohexene hydrogenation reporter reaction method previously developed and applied to solution-nanoparticle formation. The observed sigmoidal supported-nanoparticle heterogeneous catalyst formation kinetics, starting from the Ir(1,5-COD)Cl/γ-Al_2O_3 precatalyst, are closely fit by the two-step mechanism of slow continuous nucleation (A → B, rate constant $k_1 = 1.5(1.1) \times 10^{-3}$ h^{-1}) followed by fast autocatalytic surface growth (A + B → 2B, rate constant $k_2 = 1.6(2) \times 10^4$ h^{-1} M^{-1}), where A is the Ir(1,5-COD)Cl/γ-Al_2O_3 precatalyst and B is the resultant $Ir(0)_n/\gamma$-Al_2O_3 catalyst. The kinetics are significant in establishing the ability to monitor the formation of supported-nanoparticle heterogeneous catalysts in contact with solution. They also suggest that the nine synthetic and mechanistic insights from the two-step mechanism of nanoparticle formation in solution should now apply also to the formation of supported-nanoparticle heterogeneous catalysts in contact with solution. The results open the door for new syntheses of supported-nanoparticle heterogeneous catalysts under nontraditional, mild, and flexible conditions where supported organometallics and other precursors are in contact with solution, so that additional variables such as the solvent choice, added ligands, solution temperature, and so on can be used to control the catalyst formation steps and, ideally, the resultant supported-nanoparticle heterogeneous catalyst composition, size, and shape.

Introduction

Nanoparticles on metal-oxide supports constitute a large and important subset of heterogeneous catalysts.[1] However, the synthesis of these industrially significant catalysts is still largely empirical, Schlögl, for example, recently noted that "catalysts are currently 'prepared' rather than synthesized".[2] In addition, relatively little is known about *the mechanisms of formation* of those industrially most significant catalysts.[3,4] This dearth of mechanistic information is largely due to a lack of experimental methods that would allow researchers to follow the catalyst formation kinetics easily and in real time.[5−7] Methods to more quickly, routinely, and precisely monitor supported-nanoparticle

[†] Colorado State University.
[‡] Yeshiva University.

(1) (a) Gates, B. C. *Catalytic Chemistry*; John Wiley & Sons: New York, 1992. (b) Bartholomew, C. H., Farrauto, R. J. *Fundamentals of Industrial Catalytic Processes*, 2nd ed.; John Wiley & Sons: Hoboken, NJ, 2006.
(2) Schlögl, R.; Abd Hamid, S. B. *Angew. Chem., Int. Ed.* **2004**, *43*, 1628.
(3) Altman, M. S. *Science* **2010**, *327*, 789.
(4) Mondloch, J. E.; Bayram, E.; Finke, R. G. A Review of the Kinetics and Mechanisms of Formation of Supported-Nanoparticle Heterogeneous Catalysts, manuscript in preparation.

heterogeneous catalyst formation are expected to be significant in at least three ways: (i) mechanistically, resulting in an improved fundamental understanding of the mechanism(s) of heterogeneous catalyst formation; (ii) synthetically, allowing improved rational design and subsequent synthesis of heterogeneous catalysts, a significant challenge for the field;[8] and (iii) practically, since key catalytic properties[9]—such as selectivity,[10] activity,[9] lifetime, and stability[11]—depend on the catalyst surface composition,[12] size,[13] and structure.[10]

Hence, an important but still largely unmet goal of modern catalysis is to transfer to heterogeneous catalysis the synthetic control[14] over nanoparticle composition,[15] size,[16] and shape,[17] as well as the mechanistic insights into nanoparticle formation,[18−24] which have resulted from the modern revolution in nanocluster science. The hope is that transferring those insights will allow improved syntheses of, mechanistic understanding of, and catalysis by those composition-, shape-, and size-controlled supported-nanoparticles.

Relevant here is that surprisingly little is known for certain about the mechanisms of formation of supported-nanoparticle heterogeneous catalysts outside of high-vacuum studies (i.e., little is known about practical, "dirty/real-world" catalysts),[25−27] and there are no kinetic studies of the formation of supported catalysts in contact with solution (as performed herein). A review of the literature of the kinetics and mechanisms of heterogeneous catalyst formation will be available elsewhere,[4] and some lead papers[28−37] and points from that review are summarized in a footnote[38] for the interested reader.

Controlling the resultant nanoparticle *surface composition* is, in our opinion, the most overlooked, yet crucial, aspect of nanoparticle catalysts.[14h] The literature teaches that there is a general problem with *completely* removing stabilizing ligands

(5) Chupas, P. J.; Chapman, K. W.; Jennings, G.; Lee, P. L.; Grey, C. P. *J. Am. Chem. Soc.* **2007**, *129*, 13822.
(6) Uzun, A.; Gates, B. C. *Angew. Chem., Int. Ed.* **2008**, *47*, 9245.
(7) Mondloch, J. E.; Yan, X.; Finke, R. G. *J. Am. Chem. Soc.* **2009**, *131*, 6389.
(8) (a) Catalysis for Energy: Fundamental Science and Long Term Impacts of the U.S. Department of Energy Basic Energy Sciences Catalysis Science Programs; National Research Council, The National Academies Press: Washington, DC, 2009; accessible online at http://www.nap.edu/catalog/12532.html. (b) Basic Research Needs: Catalysis for Energy; PNNL-17214; Office of Basic Energy Sciences, U. S. Department of Energy: Washington, DC, 2007; accessible online at http://www.sc.doe.gov/bes/reports/list.html. (c) Opportunities for Catalysis in the 21st Century; Basic Energy Sciences Advisory Committee Subpanel Workshop Report, Workshop Chair Prof. J. M. White; A report from the Basic Energy Sciences Advisory Committee; Office of Basic Energy Sciences, U. S. Department of Energy: Washington, DC, 2002; accessible online at http://www.er.doe.gov/production/bes/reports/archives.html.
(9) Bell, A. T. *Science* **2003**, *299*, 1688.
(10) (a) Lee, I.; Delbecq, F.; Morales, R.; Albiter, M. A.; Zaera, F. *Nat. Mater.* **2009**, *8*, 132. (b) Somorjai, G. A.; Park, J. Y. *Angew. Chem., Int. Ed.* **2008**, *47*, 9212.
(11) Joo, S. H.; Park, J. Y.; Tsung, C.-K.; Yamada, Y.; Yang, P.; Somorjai, G. A. *Nat. Mater.* **2009**, *8*, 126.
(12) (a) Thomas, J. M.; Johnson, B. F. G.; Raja, R.; Sankar, G.; Midgley, P. A. *Acc. Chem. Res.* **2003**, *36*, 20. (b) Alayoglu, S.; Nilekar, A. U.; Mavrikakis, M.; Eichhorn, B. *Nat. Mater.* **2008**, *7*, 333. (c) Stowell, C. A.; Korgel, B. A. *Nano Lett.* **2005**, *5*, 1203.
(13) Che, M.; Bennett, C. O. *Adv. Catal.* **1989**, *36*, 55.
(14) Some of the more recent reviews detailing syntheses of transition metal nanoparticles include the following: (a) Aiken, J. D., III; Finke, R. G. *J. Mol. Catal. A: Chemical* **1999**, *145*, 1. (b) Crooks, R. M.; Zhao, M.; Sun, L.; Chechik, V.; Yeung, L. K. *Acc. Chem. Res.* **2001**, *34*, 181. (c) Bönnemann, H.; Richards, R. M. *Eur. J. Inorg. Chem.* **2001**, 2455. (d) Roucoux, A.; Schulz, J.; Patin, H. *Chem. Rev.* **2002**, *102*, 3757. (e) Cushing, B. L.; Kolesnichenko, V. L.; O'Connor, C. J. *Chem. Rev.* **2004**, *104*, 3893. (f) Astruc, D.; Lu, F.; Aranzaes, J. R. *Angew. Chem., Int. Ed.* **2005**, *44*, 7852. (g) Wilcoxon, J. P.; Abrams, B. L. *Chem. Soc. Rev.* **2006**, *35*, 1162. (h) Ott, L. S.; Finke, R. G. *Coord. Chem. Rev.* **2007**, *251*, 1075. (i) Semagina, N.; Kiwi-Minsker, L. *Catal. Rev.* **2009**, *51*, 147.
(15) (a) Mednikov, E. G.; Jewell, M. C.; Dahl, L. F. *J. Am. Chem. Soc.* **2007**, *129*, 11619–11630, and extensive references therein for similar nanosized clusters. (b) Jadzinsky, P. D.; Calero, G.; Ackerson, C. J.; Bushnell, D. A.; Kornberg, R. D. *Science* **2007**, *318*, 430. (c) Zhu, M.; Aikens, C. M.; Hollander, F. J.; Schatz, G. C.; Jin, R. *J. Am. Chem. Soc.* **2008**, *130*, 5883. Other non-atomically precise but compositionally well-understood nanoparticles are known and have been reviewed.[14a].
(16) Corain, B., Schmid, G., Toshima, N., Eds. *Metal Nanoclusters in Catalysis and Materials Science: The Issue of Size Control*; Elsevier: Amsterdam, 2008.
(17) (a) Ahmadi, T. S.; Wang, Z. L.; Green, T. C.; Henglein, A.; El-Sayed, M. A. *Science* **1996**, *272*, 1924. (b) Burda, C.; Chen, X.; Narayanan, R.; El-Sayed, M. A. *Chem. Rev.* **2005**, *105*, 1025. (c) Tao, A. R.; Habas, S.; Yang, P. *Small* **2008**, *4*, 310. (d) Xia, Y.; Xiong, Y.; Lim, B.; Skrabalak, S. E. *Angew. Chem., Int. Ed.* **2009**, *48*, 60.
(18) Watzky, M. A.; Finke, R. G. *J. Am. Chem. Soc.* **1997**, *119*, 10382.
(19) Hornstein, B. J.; Finke, R. G. *Chem. Mater.* **2004**, *16*, 139; see also *Chem. Mater.* **2004**, *16*, 3972.
(20) Besson, C.; Finney, E. E.; Finke, R. G. *J. Am. Chem. Soc.* **2005**, *127*, 8179.
(21) Besson, C.; Finney, E. E.; Finke, R. G. *Chem. Mater.* **2005**, *17*, 4925.
(22) Finney, E. E.; Finke, R. G. *Chem. Mater.* **2008**, *20*, 1956.
(23) For a few selected additional recent references to the growing mechanistic insights into the synthesis of nanoparticles from the modern revolution in nanocluster science, see: (a) Zheng, H.; Smith, R. K.; Jun, Y.-W.; Kisielowski, C.; Dahmen, U.; Alivisatos, A. P. *Science* **2009**, *324*, 1309. (b) Murray, C. B. *Science* **2009**, *324*, 1276. (c) Harada, M.; Inada, Y. *Langmuir* **2009**, *25*, 6049. (d) Polte, J.; Ahner, T. T.; Delissen, F.; Sokolov, S.; Emmerling, F.; Thünemann, A. F.; Kraehnert, R. *J. Am. Chem. Soc.* **2010**, *132*, 1296. (e) Polte, J.; Erler, R.; Thünemann, A. F.; Sokolov, S.; Ahner, T. T.; Rademann, K.; Emmerling, F.; Kraehnert, R. *ACS Nano* **2010**, *4*, 1076.
(24) Finney, E. E.; Finke, R. G. *J. Colloid Interface Sci.* **2008**, *317*, 351.
(25) The model UHV literature related to heterogeneous catalyst formation is extensive. For key reviews of that literature, see: (a) Venables, J. A. *Philos. Mag.* **1973**, *27*, 697. (b) Venables, J. A.; Spiller, G. D. T.; Hanbücken, M. *Rep. Prog. Phys.* **1984**, *47*, 399. (c) Poppa, H. *Catal. Rev.-Sci. Eng.* **1993**, *35*, 359. (d) Campbell, C. T. *Surf. Sci. Rep.* **1997**, *27*, 1. (e) Henry, C. R. *Vacuum* **1998**, *50*, 157. (f) Henry, C. R. *Surf. Sci. Rep.* **1998**, *31*, 231. (g) Bäumer, M.; Freund, H.-J. *Prog. surf. Sci.* **1999**, *61*, 127. (h) Henry, C. R. *Chem. Phys. Solid Surf.* **2003**, *11*, 247.
(26) (a) Goodman, D. W. *J. Phys. Chem.* **1996**, *100*, 13090. (b) Gunter, P. L. J.; Niemantsverdriet, J. W.; Ribeiro, F. H.; Somorjai, G. A. *Catal. Rev.-Sci. Eng.* **1997**, *39*, 77. (c) Ertl, G.; Freund, H.-J. *Phys. Today* **1999**, *52*, 32. (d) Freund, H.-J.; Kuhlenbeck, H.; Libuda, J.; Rupprechter, G.; Bäumer, M.; Hamann, H. *Top. Catal.* **2001**, *15*, 201. (e) van Santen, R. A.; Neurock, M. *Molecular Heterogeneous Catalysis*; Wiley-VCH: Weinheim, 2006. (f) Imbihl, R.; Behm, R. J.; Schlögl, R. *Phys. Chem. Chem. Phys.* **2007**, *9*, 3459.
(27) Thomas, J. M. *J. Chem. Phys.* **2008**, *128*, 182502.
(28) Dalla Betta, R. A.; Boudart, M. *Fifth Annual International Congress on Catalysis*; North-Holland: Palm Beach, FL, 1972; p 1329.
(29) (a) Tzou, M. S.; Sachtler, W. M. H. *Catalysis* **1987**, *38*, 233. (b) Homeyer, S. T.; Sachtler, W. M. H. *J. Catal.* **1989**, *118*, 266.
(30) Oudenhuijzen, M. K.; Kooyman, P. J.; Tappel, B.; van Bokhoven, J. A.; Koningsberger, D. C. *J. Catal.* **2002**, *205*, 135.
(31) (a) Okumura, K.; Honma, T.; Hirayama, S.; Sanada, T.; Niwa, M. *J. Phys. Chem. C* **2008**, *112*, 16740. (b) Okumura, K.; Matsui, H.; Sanada, T.; Arao, M.; Honma, T.; Hirayama, S.; Niwa, M. *J. Catal.* **2009**, *265*, 89.
(32) Wang, Y.; Xu, X.; Tian, Z.; Zong, Y.; Cheng, H.; Lin, C. *Chem.—Eur. J.* **2006**, *12*, 2542.
(33) When a $Ir(C_2H_4)_2$·zeolite precatalyst was placed under H_2, Gates and co-workers detected the formation of Ir_4 tetrahedral clusters containing both ethylidyne and di-σ-bonded ethylene by modeling the XAFS.[6] These Ir_4 clusters were shown to undergo reversible fragmentation back to the monomer Ir species upon exposure to C_2H_4 (but then back to Ir_4 under a H_2-rich atmosphere).[6] Kinetic studies of the evolution of the $Ir(C_2H_4)_2$·zeolite to Ir_4·zeolite catalyst under H_2, by the kinetic reporter reaction methods utilized herein, have proven successful in a collaborative investigation with the Gates laboratory and will be reported separately in due course.
(34) Liang, A. J.; Gates, B. C. *J. Phys. Chem. C* **2008**, *112*, 18039.

or polymers from ligand- or polymer-protected nanoparticles (i.e., ligands or polymers used during their synthesis to prevent aggregation).[39,40] This is closely related to what we have termed the "weakly ligated/labile-ligand" nanoparticle synthesis and stabilization problem;[41,42] that is, how can one prepare nanoparticles with *only* the desired, catalytically relevant ligands (or other ligands relevant to the desired physical property) present *from the start*?

Goals of the Present Studies. The overarching hypothesis of the present work is that developing the synthesis of supported-nanoparticle catalysts *formed in contact with solution*, while simultaneously studying the kinetics and mechanism under those identical conditions (i.e., in situ or ideally operando[43]), is an important way to both (a) prepare a next generation of supported-nanoparticle catalysts with composition, size, and shape control and to (b) bring what has been developed in the modern "nanoparticle revolution" [14] to supported heterogeneous catalysts and their catalysis.

On reflection, we realized it would help considerably to outline the needed studies in terms of what we define herein as a *prototype system* for the study of supported-nanoparticle heterogeneous catalysts *in contact with solution*. Specifically, a prototype system should be one in which the following eight attributes have been achieved (seven of which are reported via the present studies, vide infra): (i) a compositionally and structurally well-defined supported precatalyst is developed and employed; (ii) the system is in contact with solution, and a lower temperature reaction (at least to start) is employed with the goal of minimizing further speciation of the precatalyst;[6,36] and (iii) one both can and does establish the balanced stoichiometry of a supported-nanoparticle formation reaction to well-defined supported-nanoparticle products. In addition, a prototype system should be one in which (iv) an active and long-lived catalyst results (so that the time-consuming kinetic and mechanistic studies are worth the expense and effort); (v) a rapid, quantitative, real-time kinetic monitoring method can be applied to the forming supported-nanoparticle heterogeneous catalyst; and (vi) reproducible kinetic data are obtained so that reliable, quantitative conclusions can be drawn.[44] Ideally, (vii) a prototype system would also be one in which the supported heterogeneous catalyst system can be compared and contrasted with a kinetically and mechanistically well-studied—and ideally the prior best-studied—nanoparticle formation system in solution.[18,19,45−47] Once a prototype system is in hand, one would also like to (viii)

(35) Fierro-Gonzalez, J. C.; Gates, B. C. *J. Phys. Chem. B* **2005**, *109*, 7275.

(36) For lead references on the subject of H_2PtCl_6 speciation both in H_2O as well as in the presence of γ-Al_2O_3, see: (a) Spieker, W. A.; Liu, J.; Miller, J. T.; Kropf, A. J.; Regalbuto, J. R. *Appl. Catal. A: General* **2002**, *232*, 219. (b) Spieker, W. A.; Liu, J.; Miller, J. T.; Kropf, A. J.; Regalbuto, J. R. *Appl. Catal. A: General* **2003**, *243*, 53. (c) Shelimov, B. N.; Lambert, J.-F.; Che, M.; Didillon, B. *J. Mol. Catal. A: Chemical* **2000**, *158*, 91. (d) Mang, T.; Breitscheidel, B.; Polanek, P.; Knozinger, H. *Appl. Catal. A: General* **1993**, *106*, 239. (e) Brunelle, J. P. *Pure Appl. Chem.* **1978**, *50*, 1211. Also see footnote 29 in ref 7 for further discussion of this subject. .

(37) Schwarz, J. A.; Contescu, C.; Contescu, A. *Chem. Rev.* **1995**, *95*, 477.

(38) Our recent, comprehensive review of the relevant literature[4] reveals that studies of the formation kinetics and mechanisms of practical,[25−27] non-ultra-high-vacuum (UHV)[26a] supported-nanoparticle heterogeneous catalysts date back to the early 1970s. Specifically, (i) Boudart and co-workers systematically studied how catalyst pretreatment affected the formation of a $Pt(0)_n$/zeolite catalyst from a $Pt(NH_3)_4Cl_2$/zeolite precursor,[28] and (ii) Sachtler,[29] Koninsberger,[30] and Okumura[31] each studied the classic system $M^{II}(NH_3)_4(anion)_2$ (where M = Pt and Pd, and anion = NO_3^- and Cl^-). Other well-studied systems include (iii) H_2PtCl_6 supported on γ-Al_2O_3,[7] carbon nanotubes,[32] and TiO_2,[5] and (iv) Gates and co-workers' well-characterized $Ir(C_2H_4)_2$,[6,33] $Rh(C_2H_4)_2$,[34] and $Au(CH_3)_2$[35] supported organometallic-based precursors. Synthetically significant kinetic and mechanistic insights able to guide supported-nanoparticle heterogeneous catalyst preparation are, however, relatively rare despite such classic studies.[4] This broader lack of mechanistically guided synthetic knowledge can be attributed in large part to a lack of compositionally and structurally fully defined precatalysts (other than some notable exceptions such as Gates's systems[6,33−35]), for example, in the H_2PtCl_6 system, where multiple Pt precatalyst species exist both in the impregnation solution and on the support.[36] Furthermore, the supported-nanoparticle heterogeneous catalyst formation stoichiometry is not often established,[4] and "controlling the high-temperature treatment of nanostructures is often problematic",[2] since multiple precatalyst preparation steps such as calcination and activation are often used, but the catalyst's evolution and resultant form is rarely followed directly, further contributing to the presence of multiple precatalyst species[37] en route to the final supported-nanoparticle heterogeneous catalyst.

(39) For example, Somorjai and co-workers have made extensive efforts to remove stabilizing ligand overlayers from both $Pt(0)_n$ and $Rh(0)_n$ nanoparticles with varying—but not complete—degrees of success: (a) Rioux, R. M.; Song, H.; Hoefelmeyer, J. D.; Yang, P.; Somorjai, G. A. *J. Phys. Chem. B* **2005**, *109*, 2192. (b) Song, H.; Rioux, R. M.; Hoefelmeyer, J. D.; Komor, R.; Niesz, K.; Grass, M.; Yang, P.; Somorjai, G. A. *J. Am. Chem. Soc.* **2006**, *128*, 3027. (c) Rioux, R. M.; Hsu, B. B.; Grass, M. E.; Song, H.; Somorjai, G. A. *Catal. Lett.* **2008**, *126*, 10. (d) Borodko, Y.; Jones, L.; Lee, H.; Frei, H.; Somorjai, G. A. *Langmuir* **2009**, *25*, 6665. (e) Park, J. Y.; Aliaga, C.; Russell Renzas, J.; Lee, H.; Somorjai, G. A. *Catal. Lett.* **2009**, *129*, 1. (f) Aliaga, C.; Park, J. Y.; Yamada, Y.; Sook Lee, H.; Tsung, C.-H.; Yang, P.; Somorjai, G. A. *J. Phys. Chem. C* **2009**, *113*, 6150. (g) Grass, M. E.; Joo, S. H.; Zhang, Y.; Somorjai, G. A. *J. Phys. Chem. C* **2009**, *113*, 8616. (h) Borodko, Y. G.; Lee, H. Y.; Joo, S. H.; Zhang, Y.; Somorjai, G. A. *J. Phys. Chem. C* **2010**, *114*, 1117. (i) Kuhn, J. N.; Tsung, C.-H.; Huang, W.; Somorjai, G. A. *J. Catal.* **2009**, 209.

(40) Lee, I.; Morales, R.; Albiter, M. A.; Zaera, F. *Proc. Natl. Acad. Sci. U.S.A.* **2008**, *105*, 15241.

(41) More specifically, the "weakly ligated/labile-ligand" problem is simply the need for the efficient syntheses of nanoparticles with ideally 100% removable or replaceable ligands by using only the desired reactants (or solvent) for the reaction of choice. Others have worked on related concepts, such as "naked nanoclusters": (a) Schmid, G.; Meyer-Zaika, W.; Pungin, R.; Sawitowski, T.; Majoral, J.-P.; Caminade, A.-M.; Turrin, C.-O. *Chem.—Eur. J.* **2000**, *6*, 1693. (b) Evanoff, D. D.; Chumanov, G. *J. Phys. Chem. B* **2004**, *108*, 13948. For studies of putatively "solvent-only" stabilized nanoclusters, see: (c) Ott, L. S.; Finke, R. G. *Inorg. Chem.* **2006**, *45*, 8382, and references therein. See also our recent review on nanocluster stabilizers[14h] that further details the use of anion-free metal precursors that, in principle, can generate "weakly ligated/labile-ligand" or "solvent-only" stabilized nanoclusters. One example is the important work by Chaudret and co-workers using the precursor Ru(COD)(COT): (d) Vidoni, O.; Philippot, K.; Amiens, C.; Chaudret, B.; Balmes, O.; Malam, J.-O.; Bovin, J.-O.; Senocq, F.; Casanove, M.-J. *Angew. Chem., Int. Ed.* **1999**, *38*, 3736. (e) Pelzer, K.; Vidoni, O.; Philippot, K.; Chaudret, B.; Colliere, V. *Adv. Funcy. Mater.* **2003**, *13*, 118. For studies using $Pd_2(dba)_3$, see: (f) Dhas, N. A.; Cohen, H.; Gedanken, A. *J. Phys. Chem. B* **1997**, *101*, 6384.

(42) For our efforts to date on the "weakly ligated/labile-ligand" nanocluster catalysts concept, see: (a) Özkar, S.; Finke, R. G. *J. Am. Chem. Soc.* **2005**, *127*, 4800, where an active and selective neat-acetone reduction catalyst and only HCl plus cyclooctane are formed from $[Ir(1,5\text{-}COD)Cl]_2$ under H_2. (b) Bayram, E.; Zahmakiran, M.; Özkar, S.; Finke, R. G. In-Situ Formed "Weakly Ligated/Labile Ligand" Ir(0) Nanoparticles and Aggregates as Catalysts for the Complete Hydrogenation of Neat Benzene at Room Temperature and Mild Pressures, *Langmuir*, **2010**, in press. For a lead reference to putative "solvent-only stabilized" nanoclusters, see: (c) Ott, L. S.; Finke, R. G. *Inorg. Chem.* **2006**, *45*, 8382. (d) See also pp 1093−1094 in our review on nanocluster stabilization[14h] for putative "solvent only stabilized nanoclusters".

(43) The term "operando" is from the Latin for "working" or "operating": (a) Thomas, J. M.; Somorjai, G. A. *Top. Catal.* **1999**, *8*, preface. (b) Weckhuysen, B. M. *Chem. Commun.* **2002**, 97. (c) Guerrero-Pérez, M. O.; Bañares, M. A. *Chem. Commun.* **2002**, 1292. (d) Meunier, F.; Daturi, M. *Catal. Today* **2006**, *113*, 1.

(44) (a) Lin, Y.; Finke, R. G. *J. Am. Chem. Soc.* **1994**, *116*, 8335. (b) Lin, Y.; Finke, R. G. *Inorg. Chem.* **1994**, *33*, 4891.

(45) Ott, L. S.; Hornstein, B. J.; Finke, R. G. *Langmuir* **2006**, *22*, 9357.

(46) Aiken, J. D., III; Finke, R. G. *J. Am. Chem. Soc.* **1998**, *120*, 9545.

(47) (a) Özkar, S.; Finke, R. G. *J. Am. Chem. Soc.* **2002**, *124*, 5796. (b) Ott, L. S.; Finke, R. G. *J. Nanosci. Nanotechnol.* **2008**, *8*, 1551. (c) Ott, L. S.; Finke, R. G. *Chem. Mater.* **2008**, *20*, 2592.

Scheme 1. Cyclohexene Reporter Reaction Employed Herein To Follow $Ir(0)_n/\gamma\text{-}Al_2O_3$ Supported-Nanoparticle Heterogeneous Catalyst Formation in Contact with Solution[a] and the Two-Step Mechanism Hypothesis That Will Be Tested Herein[b]

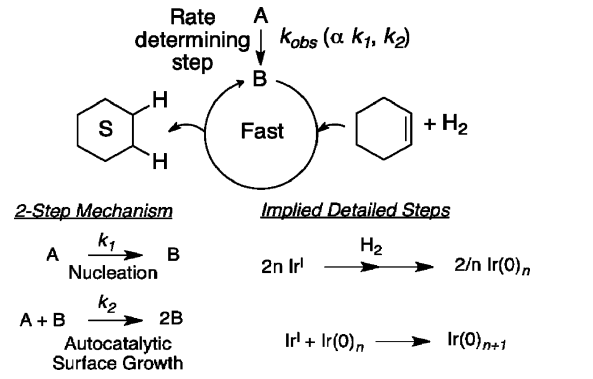

[a] A is the $Ir(1,5\text{-COD})Cl/\gamma\text{-}Al_2O_3$ precatalyst and B is the growing $Ir(0)_n$ surface. [b] See Figure 6, vide infra.

systematically vary key synthetic variables such as the support, solvent, and metal precursor to reveal their effects on the kinetics, mechanism(s) and synthesis of supported-nanoparticle heterogeneous catalyst formation in contact with solution.

Herein we describe our initial studies (a) synthesizing and characterizing a prototype system consisting of a compositionally and structurally well-defined $Ir(1,5\text{-COD})Cl/\gamma\text{-}Al_2O_3$ precatalyst; (b) characterizing the $Ir(0)_n/\gamma\text{-}Al_2O_3$ product formed in contact with solution and under H_2 and cyclohexene reduction catalysis while also establishing a balanced nanocluster formation reaction; and (c) determining the high activity and long lifetime of the resultant "weakly ligated/labile-ligand" [41] supported-nanoparticle catalyst, in which the $\gamma\text{-}Al_2O_3$ support, the solvent, and the desired reactants H_2 and cyclohexene are the *only ligands present* (since the reaction product HCl is a very poor ligand at best). Significantly, also provided are studies (d) successfully monitoring the nanocluster formation kinetics by our now well-precedented cyclohexene reporter reaction method (Scheme 1, top),[18−22,45,48,49] plus the appropriate control studies to ensure that the reporter reaction is performing reliably. Additionally provided are (e) evidence that the observed kinetic data are well-fit by a two-step mechanism of nanoparticle formation[18] in Scheme 1, plus (f) interesting comparative studies of the $[Ir(1,5\text{-COD})Cl]_2$ precursor alone, that is, in the absence of $\gamma\text{-}Al_2O_3$, which reveal the role of the solid-support in stabilizing the resultant $Ir(0)_{\sim 900}$ nanoclusters toward subsequent aggregation.

Overall, the results presented herein satisfy the first seven of the eight attributes defined above for a prototype system for kinetic and mechanistic studies of supported-nanoparticle formation in contact with solution. As such, they begin to test the global hypothesis underlying this work: that quantitative studies of the kinetics and mechanisms of heterogeneous catalyst formation *in contact with solution*[4] will allow exploration of an important, but to-date little investigated, sub-area of heterogeneous catalyst synthesis[50] and the associated mechanistic studies and resultant knowledge. A key sub-hypothesis is that the necessary prototype systems must begin with well-defined, speciation-controlled precatalysts, while also demonstrating a balanced stoichiometry to an also well-characterized, ideally highly active catalyst. The overall goal is to use the resultant knowledge to guide new and improved syntheses of better composition-, size-, and shape-controlled supported-nanoparticle heterogeneous catalysts.

Results and Discussion

$Ir(1,5\text{-COD})Cl/\gamma\text{-}Al_2O_3$: Precatalyst Synthesis and Characterization. Organometallic complexes such as $[M(1,5\text{-COD})Cl]_2$ (where M = Ir or Rh) provide a precedented[51] avenue for the preparation of well-defined oxide-supported-metal complexes.[52] They also have served as precursors for discrete polyoxoanion oxide-supported organometallics such as $[M(1,5\text{-COD})\cdot P_2W_{15}Nb_3O_{62}]^{8-}$ (M = Ir or Rh)[44,46] that evolve under H_2 and cyclohexene to the highly active,[44] yet stable and isolable,[44] as well as kinetically and mechanistically well-characterized,[18,19,45−47] soluble $Ir(0)_{\sim 300}\cdot(P_2W_{15}Nb_3O_{62}{}^{8-})_n{}^{-8n}$ nanoclusters.

For what follows, unless stated otherwise, a 2.0 wt % $Ir(1,5\text{-COD})Cl/\gamma\text{-}Al_2O_3$ precatalyst was prepared and employed in a drybox by the addition of acidic $\gamma\text{-}Al_2O_3$ to an ethyl acetate solution of $[Ir(1,5\text{-COD})Cl]_2$ of the appropriate wt % (Scheme 2, top). The solid was then brought to dryness under vacuum, as described in the Experimental Section. The resultant precatalyst is denoted $Ir(1,5\text{-COD})Cl/\gamma\text{-}Al_2O_3$, consistent with our characterization data, vide infra.

The Ir content of the $Ir(1,5\text{-COD})Cl/\gamma\text{-}Al_2O_3$ precatalyst was confirmed by inductively coupled plasma optical emission spectroscopy (ICP-OES): theoretical 1.1% Ir, found 1.0% Ir. In addition, we find that 1 equiv of cyclooctadiene per Ir is

(48) Aiken, J. D., III; Finke, R. G. *Chem. Mater.* **1999**, *11*, 1035.
(49) Widegren, J. A.; Aiken, J. D., III; Özkar, S.; Finke, R. G. *Chem. Mater.* **2001**, *13*, 312.

(50) Traditional heterogeneous catalyst synthesis is most often carried out via a gas−solid system and interface. In the present work, the supported-nanoparticle synthesis occurs in a solid−liquid system, a less common but not unprecedented synthetic method. For leading references to prior examples, see: (a) De Jong, K. P.; Geus, J. W. *Appl. Catal. A: General* **1982**, *4*, 41. (b) Bond, G. C.; Rawle, A. F. *J. Mol. Catal. A: Chemical* **1996**, *109*, 261. (c) Sales, E. A.; Benhamida, B.; Caizergues, V.; Lagier, J.-P.; Fiévet, F.; Bozon-Verduraz, F. *Appl. Catal. A: General* **1998**, *172*, 273. (d) Bonet, F.; Grugeon, S.; Urbina, R. H.; Tekaia-Elhsissen, K.; Tarascon, J.-M. *Solid State Sci.* **2002**, *4*, 665. (e) Hulea, V.; Brunel, D.; Galarneau, A.; Philippot, K.; Chaudret, B.; Kooyman, P. J.; Fajula, F. *Microporous Mesoporous Mater.* **2005**, *79*, 185. (f) Zawadzki, M.; Okal, J. *Mater. Res. Bull.* **2008**, *43*, 3111. (g) Boutros, M.; Denicourt-Nowicki, A.; Roucoux, A.; Gengembre, L.; Beaunier, P.; Gédéon, A.; Launay, F. *Chem. Commun.* **2008**, 2920. (h) Xie, Y.; Ding, K.; Liu, Z.; Tao, R.; Sun, Z.; Zhang, H.; An, G. *J. Am. Chem. Soc.* **2009**, *131*, 6648. (i) Polisski, S.; Goller, B.; Wilson, K.; Kovalev, D.; Zaikowskii, V.; Lapkin, A. *J. Catal.* **2010**, *271*, 59.
(51) (a) Esteban, P.; Real, J.; Bayon, J. C.; Dexpert, H.; Bazin, D.; Maire, G. *J. Organomet. Chem.* **1988**, *356*, 113. (b) Esteban, P.; Real, J.; Bayon, J. C.; Dexpert, H.; Bazin, D.; Garin, F.; Girard, P.; Maire, G. *J. Chim. Phys.* **1989**, *86*, 1778. (c) Vierkötter, S. A.; Barnes, C. E.; Hatmaker, T. L.; Penner-Hahn, J. E.; Stinson, C. M.; Huggins, B. A.; Benesi, A.; Ellis, P. D. *Organometallics* **1991**, *10*, 3803. (d) Barnes, C. E.; Ralle, M.; Vierkötter, S. A.; Penner-Hahn, J. E. *J. Am. Chem. Soc.* **1995**, *117*, 5861.
(52) (a) Esteban et al. studied a similar $[Ir(1,5\text{-COD})Cl]_2$ plus $\gamma\text{-}Al_2O_3$ supported-metal complex,[51] but did not emphasize the supported-nanoparticle heterogeneous catalyst formation steps or kinetics and mechanism. (b) Of interest and potential broader significance is that the precatalyst structure determined herein is *different* than that reported by Esteban et al.[51a,b] Those authors synthesized 2.5 wt % $[Ir(1,5\text{-COD})Cl]_2$ on $\gamma\text{-}Al_2O_3$ via deposition from CH_2Cl_2 (e.g., vs the deposition from ethyl acetate employed herein) and then used CO trapping/IR plus EXAFS spectroscopy en route to proposing an "$[Ir(1,5\text{-COD})(\mu\text{-}O_{Support})]_2$" dimeric structure. Two possible interpretations of the different finding of our and their ostensibly closely analogous studies are that (i) seemingly minor modifications in the precatalyst synthesis protocol (e.g., just the deposition solvent) or differences in the $\gamma\text{-}Al_2O_3$ support (e.g., perhaps its H_2O content; they dried theirs at 200 °C and 10^{-3} Torr, while we dried ours at 160 °C and 1 atm) can yield significant differences in the resultant precatalyst composition and structure, or (ii) one (or both) of the structural studies contains some at present undetected error in the analysis.

Scheme 2. Synthesis of the Ir(1,5-COD)Cl/γ-Al_2O_3 Precatalyst (Top) as Well as the CO Trapping Reaction for Subsequent IR Analysis (Bottom)

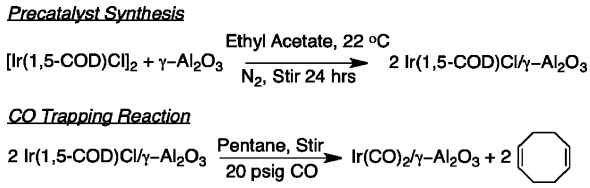

converted into 1 equiv of cyclooctane (i.e., the expected amount) by the end of the supported-nanoparticle heterogeneous catalyst formation reaction, vide infra. This result suggests that an intact $Ir^I(1,5\text{-}COD)^+$ moiety is present on the γ-Al_2O_3 support, consistent with a 16-electron Ir(I) species and its strong preference for a square planar geometry.

One precedent, valuable method for probing the nature of low-valent supported-metal complexes is to place the precatalyst under CO (Scheme 2, bottom), isolate the resultant material (a beige solid), and examine its IR spectrum in the CO stretch region.[53] The IR spectrum in Figure 1 (green line) shows ν(CO) stretches at 2076 and 2000 cm^{-1}, as expected for the symmetric and antisymmetric stretches, respectively, of a C_{2v}-symmetric $Ir^I(CO)_2/\gamma$-Al_2O_3 dicarbonyl species.[54] As a control, an authentic $Ir^I(CO)_2/\gamma$-Al_2O_3 dicarbonyl precatalyst sample was prepared by contacting $Ir^I(CO)_2$(acac) with γ-Al_2O_3, revealing very similar bands at 2075 and 1998 cm^{-1} (Figure 1, red line), confirming the assignment of a supported $Ir(CO)_2^+$ moiety. Note that the presence of only two CO bands in the IR spectrum *is consistent with the [Ir(1,5-COD)Cl]$_2$ dimer being split into the corresponding Ir(1,5-COD)Cl monomer during its support on γ-Al_2O_3*; if a dimeric [Ir(1,5-COD)μ-$O_{Support}$]$_2$ species had been present, then symmetry considerations along with literature precedent[51] suggest that three CO bands would have been seen (i.e., in that case arising from the coupling of the *cis*-$Ir(CO)_2$ moieties[55]). Precedent for surface-induced cleavage of the bridging M−Cl bonds has been observed for the deposition of [Rh(1,5-COD)Cl]$_2$ onto partially dehydroxylated γ-Al_2O_3.[52]

X-ray absorption near-edge structure (XANES) and extended X-ray absorption fine structure (EXAFS) analyses were used to further probe the nature of the precatalyst structure and, ultimately, provide further strong support for a Ir(1,5-COD)Cl/γ-Al_2O_3 precatalyst composition and structure. The XANES spectrum of the Ir(1,5-COD)Cl/γ-Al_2O_3 precatalyst is shown

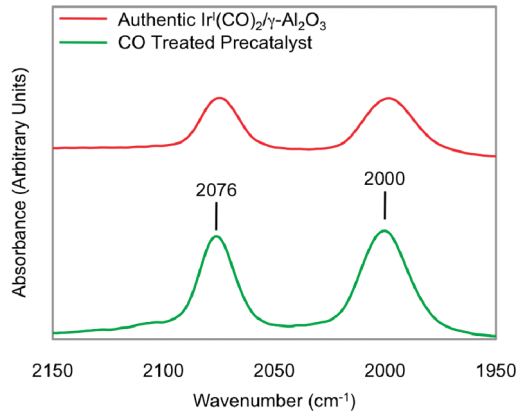

Figure 1. IR spectra of the Ir(1,5-COD)Cl/γ-Al_2O_3 precatalyst after reaction with CO (green line), ν(CO) = 2076 and 2000 cm^{-1}, consistent with the assignment of $Ir(CO)_2/\gamma$-Al_2O_3. The red line is a sample of independently prepared $Ir(CO)_2/\gamma$-Al_2O_3, ν(CO) = 2075 and 1998 cm^{-1}.

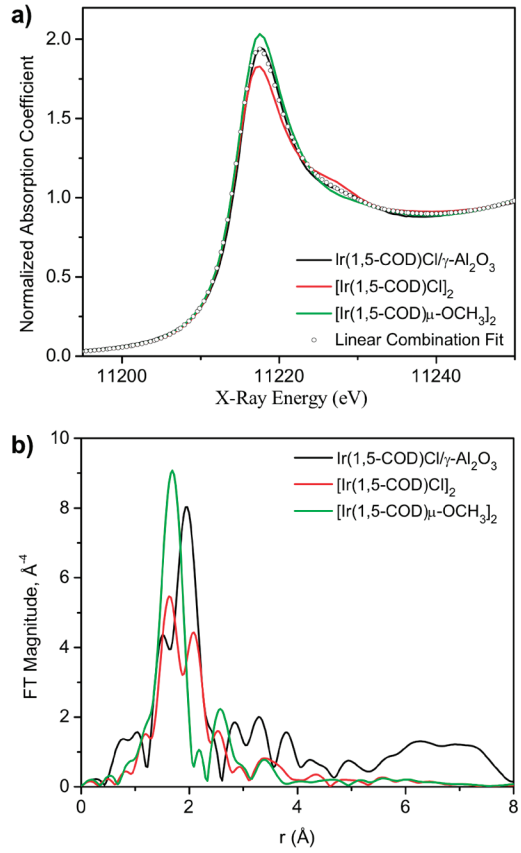

Figure 2. XAFS data comparison of the precatalyst Ir(1,5-COD)Cl/γ-Al_2O_3 to the reference compounds [Ir(1,5-COD)Cl]$_2$ and [Ir(1,5-COD)μ-OCH_3]$_2$: (a) XANES spectra and (b) EXAFS data (Fourier transform magnitude of $k^3\chi(k)$; k ranges 2−11.5 $Å^{-1}$). Error bars for the resultant coordination numbers are provided in Table 1.

in Figure 2a, in comparison to those of the well-known [Ir(1,5-COD)Cl]$_2$[56] and [Ir(1,5-COD)μ-OCH_3]$_2$[57] reference compounds. The position and intensity as well as the shape of the Ir L_3-edge white-line are consistent with the precatalyst structure being formally in the Ir^I oxidation state (the white-line at the L_3-edge is an element-specific quantum mechanical transition arising from the excitation of core-level $2p_{3/2}$ electrons into unoccupied $5d_{5/2}$ and $5d_{3/2}$ states above the Fermi level[58]). In addition, the white-line intensity of the Ir(1,5-COD)Cl/γ-Al_2O_3 precatalyst is intermediate between those of the [Ir(1,5-COD)Cl]$_2$ and [Ir(1,5-COD)μ-OCH_3]$_2$ reference compounds. This suggests partial substitution of the chloride ligands from the [Ir(1,5-COD)Cl]$_2$ precursor with an oxo-type ligand, an −OH from the γ-Al_2O_3 support being consistent with all of our evidence,

(53) (a) Rice, C. A.; Worley, S. D.; Curtis, C. W.; Guin, J. A.; Tarrer, A. R. *J. Chem. Phys.* **1981**, *74*, 6487. (b) van't Blik, H. F. J.; van Zon, J. B. A. D.; Huizinga, T.; Koningsberger, D. C.; Prins, R. *J. Am. Chem. Soc.* **1985**, *107*, 3139. (c) Frank, M.; Bäumer, M.; Kühnemuth, R.; Freund, H.-J. *J. Phys. Chem. B* **2001**, *105*, 8569.
(54) (a) Kawi, S.; Chang, J.-R.; Gates, B. C. *J. Phys. Chem.* **1993**, *97*, 5375. (b) Zhao, A.; Gates, B. C. *Langmuir* **1997**, *13*, 4024.
(55) (a) Roberto, D.; Cariati, E.; Psaro, R.; Ugo, R. *Organometallics* **1994**, *13*, 4227. (b) Bullitt, J. G.; Cotton, F. A. *Inorg. Chim. Acta* **1971**, *5*, 637. (c) Lawson, D. N.; Wilkinson, G. *J. Chem. Soc.* **1965**, 1900.
(56) (a) Crabtree, R. H.; Morris, G. E. *J. Organomet. Chem.* **1977**, *135*, 395. (b) Cotton, F. A.; Lahuerta, P.; Sanau, M.; Schwotzer, W. *Inorg. Chim. Acta* **1986**, *120*, 153.
(57) (a) Uson, R.; Oro, L. A.; Cabeza, J. A. *Inorg. Syn.* **1985**, *23*, 126. (b) Green, M.; Kuc, T. A.; Taylor, S. H. *J. Chem. Soc. (A) Inorg. Phys.* **1971**, 2334.
(58) Rehr, J. J.; Albers, R. C. *Rev. Mod. Phys.* **2000**, *72*, 621.

Table 1. Best-Fit Results Obtained via EXAFS Analysis for Ir Black, Ir(0)$_{\sim 900}$/γ-Al_2O_3, Precatalyst Ir(1,5-COD)Cl/γ-Al_2O_3, and Reference Compounds $[Ir(1,5\text{-COD})Cl]_2$ and $[Ir(1,5\text{-COD})\mu\text{-}OCH_3]_2$[a]

	sample				
	Ir black	Ir(0)$_{\sim 900}$/γ-Al_2O_3	Ir(1,5-COD)Cl/γ-Al_2O_3	$[Ir(1,5\text{-COD})Cl]_2$	$[Ir(1,5\text{-COD})\mu\text{-}OCH_3]_2$
N_{Ir-Ir}	12[b]	9.2(2.8)			
N_{Ir-Cl}			2.4(7)[c]	1.9(5)[c]	
N_{Ir-C}			3.6(7)	4.1(5)	4[d]
N_{Ir-O}					2[d]
$N_{Ir\text{-}Total}$			6[c]	6[c]	6
R_{Ir-Ir} (Å)	2.713(3)	2.68(2)			
R_{Ir-Cl} (Å)			2.36(1)	2.41(1)	
R_{Ir-C} (Å)			2.07(3)	2.10(1)	2.05(3)
R_{Ir-O} (Å)					2.07(1)
σ^2_{Ir-Ir} (Å^2)	0.0032(1)	0.0042(27)			
σ^2_{Ir-Cl} (Å^2)			0.0031(16)	0.0048(19)	
σ^2_{Ir-C} (Å^2)			0.0056(19)	0.0039(12)	0.0076(42)
σ^2_{Ir-O} (Å^2)					0.0008(5)

[a] The actual fits are shown in the Supporting Information. [b] N_{Ir-Ir} is fixed at 12, based on the crystallographically determined structure. [c] $N_{Ir\text{-}Total}$ is fixed at 6, and N_{Ir-Cl} is constrained to vary as $6 - N_{Ir-C}$. [d] N_{Ir-O} and N_{Ir-C} are fixed at 2 and 4, respectively, based on the known structure of this reference compound.[57]

vide infra. This qualitative result was further confirmed by simulating the Ir(1,5-COD)Cl/γ-Al_2O_3 precatalyst spectrum as a linear combination of the $[Ir(1,5\text{-COD})Cl]_2$ and $[Ir(1,5\text{-COD})\mu\text{-}OCH_3]_2$ model compounds (Figure 2a, black circles): the precatalyst spectrum is well modeled by 47% $[Ir(1,5\text{-COD})Cl]_2$ plus 53% $[Ir(1,5\text{-COD})\mu\text{-}OCH_3]_2$, *consistent with an Ir(1,5-COD)Cl/γ-Al_2O_3 structure in which the fourth ligand at Ir is an −OH or other overall neutral oxygen ligand donated by the γ-Al_2O_3 support.*

EXAFS was used to further elucidate the coordination environment around Ir in the Ir(1,5-COD)Cl/γ-Al_2O_3 precatalyst. The Fourier-transformed, k^3-weighted Ir-L_3 EXAFS data are plotted in Figure 2b, again alongside the data for the two Ir reference compounds. Two distinct peaks at ∼1.6 and ∼2.1 Å are present in the $[Ir(1,5\text{-COD})Cl]_2$ reference spectrum due to the Ir−C (i.e., cyclooctadiene ligand) and Ir−Cl scattering contributions. Each EXAFS spectrum was fit using theoretical signals modeled with FEFF6[59] (see the Supporting Information). The data were analyzed in the first nearest neighbor (hereafter 1NN) distance range only; details of the analysis are provided in the Experimental Section. The best-fit values of the 1NN structural parameters are listed in Table 1. The 1NN scattering parameter for $[Ir(1,5\text{-COD})Cl]_2$, $N_{Ir\text{-}total}$, was constrained to 6 and yielded coordination numbers for Ir−C and Ir−Cl of 4.1 ± 0.5 and 1.9 ± 0.5, respectively. In contrast, only one dominant scattering peak is present at ∼1.7 Å for the $[Ir(1,5\text{-COD})\mu\text{-}OCH_3]_2$ reference spectrum, arising from both the C (from cyclooctadiene) and O (from the bridging methoxy ligands) scatterers since EXAFS is unable to distinguish between the two.

The Ir(1,5-COD)Cl/γ-Al_2O_3 precatalyst also contains split peaks, due to the presence of multiple ligands in the Ir coordination sphere. The partial replacement of chloride by oxo ligands from the γ-Al_2O_3 support is believed to account for the subtle change in peak position and amplitude relative to those for the $[Ir(1,5\text{-COD})Cl]_2$ precursor. When the overall coordination number of the precatalyst structure was held constant at 6, N_{Ir-C} and N_{Ir-Cl} were found to be 3.6 ± 0.7 and 2.4 ± 0.7, respectively. In addition, theoretical modeling done without imposing such constraints (i.e., $N_{Ir\text{-}Total} = 6$) for both the precatalyst and $[Ir(1,5\text{-COD})Cl]_2$ reference compound reveals overall coordination numbers of 6.1 ± 1.5 and 5.9 ± 0.9, respectively, consistent with the literature data.[51,56] The individual Ir−C and Ir−Cl pair coordination numbers also agree with those obtained by the constrained fit model, further confirming that the CN(Ir−1NN) = 6 model is a good approximation. Pleasingly, the EXAFS and the XANES analyses *independently confirm* the presence of chloride in the first coordination shell of Ir for the Ir(1,5-COD)Cl/γ-Al_2O_3 precatalyst structure. The two techniques complement each other in this work, giving a range of possible values of the Ir−Cl coordination numbers [between 1 Ir−Cl pair per Ir (by analysis of the XANES) and 2.4 Ir−Cl pairs per Ir (by analysis of the EXAFS)], thereby constraining the possible precatalyst structural models, vide infra.

In short, XANES and EXAFS confirm the CO trapping and subsequent IR analysis results by revealing that supporting the dimeric $[Ir(1,5\text{-COD})Cl]_2$ on γ-Al_2O_3 results in splitting this precursor complex into monomeric units. The EXAFS data are consistent with the presence of six 1NN scatterers around Ir in the precatalyst structure, as one would expect for an Ir^I, d^8 square planar complex with one 1,5-COD ligand (i.e., four 1NN C scatterers), one Cl, and one other O ligand, taken to be a surface hydroxyl, −OH, by charge balance. The XANES data are also consistent with a mixed chloro and oxo ligand environment around Ir, further supported by the fit to a linear combination of the $[Ir(1,5\text{-COD})Cl]_2$ and $[Ir(1,5\text{-COD})\mu\text{-}OCH_3]_2$ model compounds. Given that EXAFS provides an average result, we cannot unequivocally rule out by the XAFS a 1:1 mixture of $Ir(1,5\text{-COD})Cl(-Cl-Al)_{Support}$ plus $Ir(1,5\text{-COD})OH(-OH)_{Support}$, although chemically this—and in a precise 1:1 ratio—seems less plausible, as do other possibilities that do not fit our structural data.[52b] Such a mixture is also less consistent with the (just) two-band $Ir(CO)_2$ IR data, vide supra. Overall, the data are fully consistent with and supportive of the precatalyst structure $Ir^I(1,5\text{-COD})Cl(-OH)_{Support}$/$\gamma$-$Al_2O_3$, designated as Ir(1,5-COD)Cl/γ-Al_2O_3.[60] Significantly, consistent with the well-defined composition and structure of our Ir(1,5-COD)Cl/γ-Al_2O_3 precatalyst, we see highly reproducible supported-nanoparticle heterogeneous catalyst formation kinetics (vide infra), results pleasingly much more "homogeneous catalysis-like" than "heterogeneous

(59) Zabinsky, S. I.; Rehr, J. J.; Ankudinov, A.; Albers, R. C.; Eller, M. J. *J. Phys. Rev. B* **1995**, *52*, 2995.

Scheme 3. Supported-Nanoparticle Heterogeneous Catalyst Formation Reaction Stoichiometry Starting from the Ir(1,5-COD)Cl/γ-Al_2O_3 Precatalyst (Top), along with the Cyclohexene Reporter Reaction (Bottom)

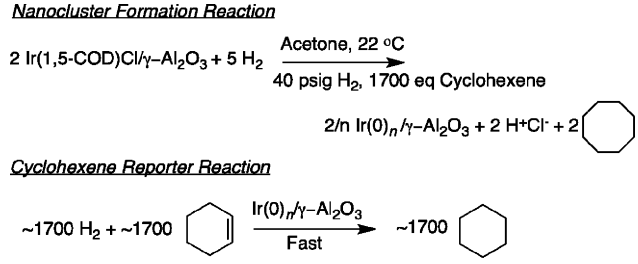

catalysis-like", probably in no small part due to control over the precatalyst speciation.

$Ir(0)_n/\gamma$-Al_2O_3 Supported-Nanoparticle Heterogeneous Catalyst Formation: Solution Synthesis, Resultant Stoichiometry, and Product Characterization. To convert the Ir(1,5-COD)Cl/γ-Al_2O_3 precatalyst into the active $Ir(0)_n/\gamma$-Al_2O_3 catalyst product, 50 mg of the precatalyst was placed in acetone along with ~1700 equiv of cyclohexene (per equivalent of Ir) (Scheme 3, top); note that the Ir(1,5-COD)Cl/γ-Al_2O_3 precatalyst is, then and therefore, in contact with acetone, cyclohexene, and H_2 only (vide infra). The mixture was sealed in a Fisher Porter (FP) bottle equipped with Swagelock Quick-Connects, removed from the drybox, placed in a temperature-regulated water bath, attached to an O_2- and H_2O-scrubbed H_2 line, interfaced to a pressure transducer (that reports ±0.01 psig), and stirred at 600 rpm, all as done previously in our well-described kinetic/synthetic apparatus.[18−22] The reduction of cyclohexene to cyclohexane serves as a reporter reaction[18−22] (Scheme 1, vide supra) that is able to monitor the formation of the $Ir(0)_n/\gamma$-Al_2O_3 catalyst, vide infra (Scheme 3, bottom). As before,[18−22] we denote these conditions as "standard conditions" in the Experimental Section and throughout the rest of the paper.

The designed Ir(1,5-COD)Cl/γ-Al_2O_3 precatalyst allows confirmation of the reaction stoichiometry (Scheme 3, top) via the evolution of the expected 1.0 equiv of cyclooctane [1.0 ± 0.1 equiv of cyclooctane per Ir evolved after approximately 1 h, as confirmed by gas−liquid chromatography (GLC), see Figure 7]. Although the uptake of 5.0 equiv of H_2 was nominally expected (Scheme 3), 6.8 ± 0.2 equiv of H_2 is consumed in the catalyst formation reaction. The additional 1.8 equiv of H_2 is very probably due to the well-known phenomenon of H_2 spillover onto the support,[61] especially since the corresponding $Ir(0)_n$ nanoparticle formation reaction in solution[44] does not take up any "extra" H_2 (so that $Ir(0)_n(H)_2$ hydride species, for example, are *not* seen, at least in the analogous $Ir(0)_n$ nanoparticle formation reaction in solution[44,62]). This is a good example of the value of studying a system in which the products, kinetics, and mechanism of the analogous $Ir(0)_n$ nanoparticle formation reaction in solution are available for comparison.[18,19,45−47] Interestingly (and in response to a reviewer's query), we note that the observed spillover (~1.8 H_2/Ir) is within 2-fold of that seen for the polyoxoanion "support" (~1 H_2/Ir) but far below spillover ratios of as high as, for example, 350 H_2/Pt seen in the literature.[61]

The dark gray $Ir(0)_n/\gamma$-Al_2O_3 products were examined by transmission electron microscopy (TEM) and high-resolution (HR) TEM (Figure 3, which also shows the associated particle size distribution), revealing well-dispersed Ir nanoparticles on the γ-Al_2O_3 support. The resultant nanoparticles are 2.9 ± 0.4 nm in diameter (i.e., ±14%, so-called near-monodisperse nanoparticles[63]), corresponding *on average* to an $Ir(0)_{\sim 900}/\gamma$-Al_2O_3 product.[64] HRTEM images confirm that the $Ir(0)_{\sim 900}$ nanoparticles present on the γ-Al_2O_3 are crystalline (at least under the TEM beam, crystallization artifacts under the TEM beam being well known[65]), with a lattice spacing of 2.21 Å, as expected for (111) Ir(0) (additional TEM images and particle size histograms are provided in the Supporting Information). Interestingly, the observed, on average $Ir(0)_{\sim 900}/\gamma$-Al_2O_3 nanoparticle products are very close to the sixth full closed-shell "magic-number-sized" clusters containing 923 atoms in the limit of those precise, magic-number-sized clusters.[66] Relevant here again is a piece of information from the $Ir(0)_n$ solution nanoparticle formation system and precedent:[66,44b] a tendency to form closed-shell ("magic number") nanoparticles is seen in solution nanocluster formation occurring by the two-step mechanism[66] shown back in Scheme 1. The reason magic-number-sized nanoparticles tend to form is because the autocatalytic surface-growth step[18,66] of the two-step mechanism produces full-shell nanoclusters "where each surface atom contains the maximum number of metal−metal bonds".[66] Hence, once magic-number clusters are formed, they are more stable and then, as a result, grow further only relatively slowly, the end result being a tendency for the more stable, magic-number-sized clusters to accumulate.[66]

The $Ir(0)_{\sim 900}/\gamma$-Al_2O_3 product was further characterized using XAFS to evaluate the electronic structure and atomic interactions of the local environment. The Ir L_3-XANES spectrum obtained for $Ir(0)_{\sim 900}/\gamma$-Al_2O_3 shows a XANES white-line comparable to that of an Ir(0) black standard in both position and amplitude, suggesting a similar electronic structure (Figure 4a). In contrast, the near-edge spectrum of the Ir(1,5-COD)Cl/γ-Al_2O_3 precatalyst features an increased white-line intensity, as well as a pronounced shift to higher energy relative to Ir black, consistent with a higher, formally Ir(I) oxidation state in comparison to

(60) A similar structure has been proposed on the basis of CO trapping/IR experiments for a different, but related, Ir^I complex supported on SiO_2,[55a] namely [Ir(cyclooctane)$_2$(HOSi≡)Cl] (where HOSi≡ is the weak interaction of the Ir with a silanol group from the silica).

(61) Conner, W. C., Jr.; Falconer, J. L. *Chem. Rev.* **1995**, *95*, 759.

(62) Aiken, J. D.; Lin, Y.; Finke, R. G. *J. Mol. Catal. A: Chemical* **1996**, *114*, 29. This paper provides evidence against Ir(0) nanocluster hydrides, $Ir(0)_n(H)_2$, as at least the catalyst resting form in solution and when placing the well-defined Ir(0) nanoparticle precursor $(Bu_4N)_5Na_3[(1,5\text{-COD})Ir{\cdot}P_2W_{15}Nb_3O_{62}]$ under H_2. The resultant Ir(0) nanopraticle formation reaction consumes 3.5(0.3) equiv of H_2, with 2.0 equiv of the observed H_2 uptake being used for the reduction of 1,5-COD to cyclooctane and 0.5 equiv H_2 for the reduction of Ir(I) to Ir(0). The additional 1.0 equiv of H_2 forms the two-electron-reduced $P_2W^{VI}{}_{13}W^{V}{}_2Nb_3O_{62}{}^{11-}$ (plus two H^+) "heteropolyblue" which further condenses to $P_4W^{VI}{}_{26}W^{V}{}_4Nb_6O_{123}{}^{20-} + H_2O$, a novel example of net $H^{\bullet}$ "spillover" onto the soluble polyoxoanion "support". Overall, the H_2 reduction stoichiometry under 40 psig H_2 demonstrates that, at least in acetone solution, just Ir(0) and no $H_xIr(0)$ hydrides are formed within experimental error.

(63) "Near monodisperse" nanoparticles are defined as ≤15% size distributions; see Aiken, J. D., III; Lin, Y.; Finke, R. G. *J. Mol. Catal. A: Chemical* **1996**, *114*, 29.

(64) Note that "$Ir(0)_{\sim 900}$" is simply a convenient nomenclature that refers to the *average* number of metal atoms in the, *on average*, 2.9 nm $Ir(0)_n$ nanoparticles. This nomenclature is not meant to imply that the nanoparticles are truly monodisperse; indeed, the 2.9 ± 0.4 nm size distribution implies that clusters ranging from $Ir_{\sim 600}$ to $Ir_{\sim 1300}$ actually exist.

(65) (a) Akita, T.; Okumura, M.; Tanaka, K.; Kohyama, M.; Haruta, M. *Catal. Today* **2006**, *117*, 62. (b) Hackett, S. F. J.; Brydson, R. M.; Gass, M. H.; Harvey, I.; Newman, A. D.; Wilson, K.; Lee, A. F. *Angew. Chem., Int. Ed.* **2007**, *46*, 8593. (c) Pyrz, W. D.; Buttrey, D. J. *Langmuir* **2008**, *24*, 11350. (d) Uzun, A.; Ortalan, V.; Hao, Y.; Browning, N. D.; Gates, B. C. *ACS Nano* **2009**, *3*, 3691.

(66) Watzky, M. A.; Finke, R. G. *Chem. Mater.* **1997**, *9*, 3083.

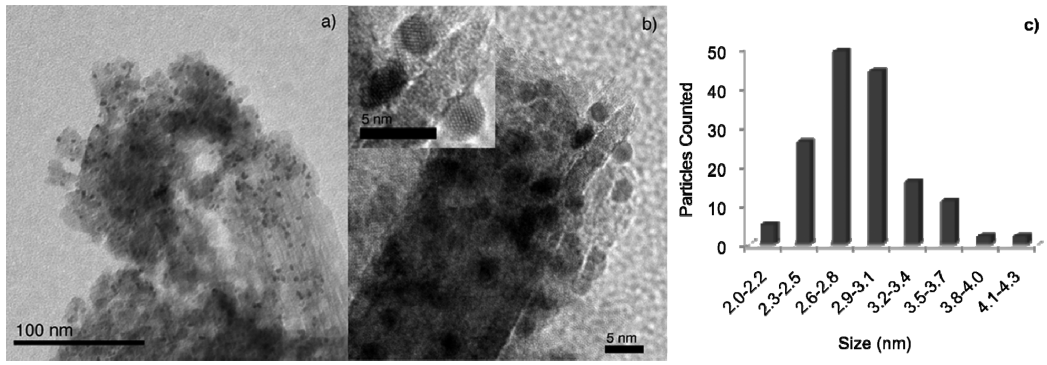

Figure 3. TEM imaging along with the associated particle size histogram of the $Ir(0)_{\sim 900}/\gamma\text{-}Al_2O_3$ catalyst. (a) A large-area view (scale bar 100 nm) showing that the nanoparticles are well dispersed on the support. (b) A close-up view (scale bar 5 nm), with the inset revealing that the Ir nanoparticles are crystalline. (c) The associated particle size histogram for the resultant $Ir(0)_{\sim 900}/\gamma\text{-}Al_2O_3$ catalyst.

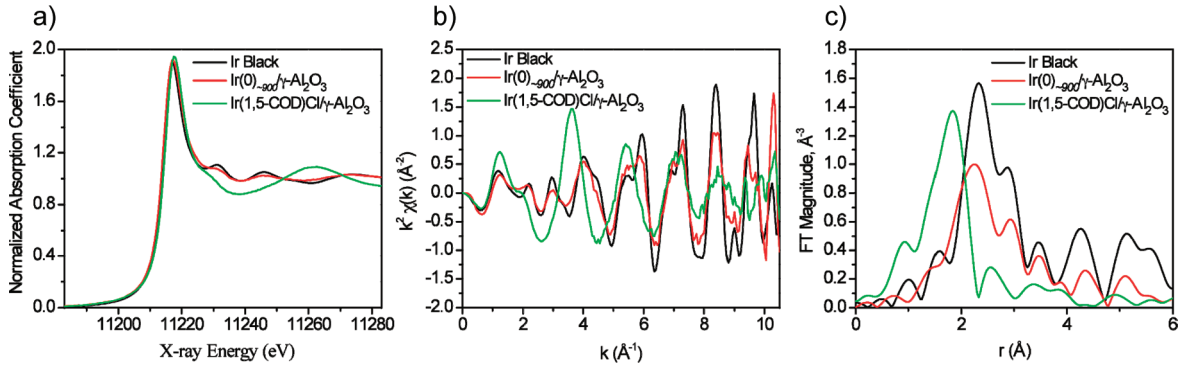

Figure 4. XAFS data for Ir black, the $Ir(0)_{\sim 900}/\gamma\text{-}Al_2O_3$ supported-nanoparticle, and $Ir(1,5\text{-COD})Cl/\gamma\text{-}Al_2O_3$ precatalyst samples: (a) XANES spectra; (b) k^2-weighted, background-subtracted EXAFS signal, $\chi(k)$; and (c) Fourier transform magnitudes of $k^2\chi(k)$ ($k = 2-10$ Å^{-1}).

the resultant $Ir(0)_{\sim 900}/\gamma\text{-}Al_2O_3$ sample. Figure 4b,c presents the background-subtracted and edge-step normalized EXAFS data in k- and r-spaces for $Ir(0)_{\sim 900}/\gamma\text{-}Al_2O_3$ in comparison to those of the $Ir(1,5\text{-COD})Cl/\gamma\text{-}Al_2O_3$ precatalyst and Ir black. The in-phase EXAFS spectra of $Ir(0)_{\sim 900}/\gamma\text{-}Al_2O_3$ and Ir black point to the metallic nature of the $\gamma\text{-}Al_2O_3$ supported $Ir(0)_{\sim 900}$ nanoparticles. Independent theoretical modeling (shown in the Supporting Information) for $Ir(0)_{\sim 900}/\gamma\text{-}Al_2O_3$ reveals a 1NN value (coordination number) of 9.2 ± 2.8 (Table 1), corresponding to an average diameter of ∼2.7 nm using the appropriate parameters for Ir,[67] fully consistent with the TEM results (2.9 ± 0.4 nm).

In summary, the supported-nanoparticle formation reaction stoichiometry of $Ir(0)_{\sim 900}$ nanoparticles on $\gamma\text{-}Al_2O_3$ shown in Scheme 3 was confirmed via cyclooctane evolution, H_2 uptake, TEM, EXAFS, and XANES. Overall, the balanced stoichiometry from a well-defined precatalyst to a well-defined supported catalyst satisfies criteria i−iii for a prototype system as defined earlier. Pleasingly, an unusually active, as well as long-lived, "weakly ligated/labile-ligand" catalyst also results, since only acetone, cyclohexene, H_2, and the support are present as possible ligands, as detailed next.

$Ir(0)_{\sim 900}/\gamma\text{-}Al_2O_3$: A Highly Coordinatively Unsaturated, and thus Highly Active and Long-Lived, Catalyst in Comparison to Literature Ir/Al_2O_3 Heterogeneous Catalysts. An important criterion (number iv, vide supra) of a prototype system is that the resultant catalyst be highly active and long-lived, in no small part to ensure that subsequent detailed kinetic and mechanistic studies are worth the effort. Hence, we examined the catalytic ability of the $Ir(0)_{\sim 900}/\gamma\text{-}Al_2O_3$ product in the test reaction of cyclohexene hydrogenation. Specifically, we examined the turnover frequency (TOF, h^{-1}) and observable total turnovers (TTOs) in comparison to those of two literature $Ir(0)_n/Al_2O_3$ catalysts previously tested in our laboratories.[44b] The results are shown in Table 2. The present $Ir(0)_{\sim 900}/\gamma\text{-}Al_2O_3$ catalyst affords 8200 (±1700) turnovers per hour and 220 000 TTOs after correcting, as one should, for the number of surface Ir atoms (calculated from the TEM data and as described in the Experimental Section). This activity exceeds by ≥2.2- to 4.8-

Table 2. Activity Comparison of Several $Ir(0)_n/Al_2O_3$ Heterogeneous Catalysts for the Reduction of Cyclohexene to Cyclohexane[a]

catalyst	TOF (turnovers/h)	TTOs (demonstrated)	ref
Exxon's 80% dispersed $Ir/\eta\text{-}Al_2O_3$	1740 ± 250[b,c]	20 000	44b
commercial 7.9% dispersed $Ir/\gamma\text{-}Al_2O_3$	3950 ± 1000[b,c]	410 000	44b
$Ir(0)_{\sim 900}/\gamma\text{-}Al_2O_3$ (∼38% dispersed)	≥8200 ± 1700[d]	≥220 000[d]	this work

[a] Each reaction was carried out at 40 psig of H_2, 22 °C, and in acetone, with stirring at 600 rpm. [b] These data are taken from D. Edlund's Ph.D. thesis from our laboratories[68] and were run in acetone, under 40 psig H_2 and 22 °C, *conditions identical to those employed herein*, with the exception that the acetone in these prior studies was dried over 3 Å molecular sieves.[44b] [c] These data are corrected for the number of available Ir atoms by H_2 chemisorption measurements. [d] The TOF as well as TTOs are corrected for the number of Ir surface atoms, which are based on calculations from the TEM data (as detailed in the Experimental section herein).

(67) Frenkel, A. I.; Hills, C. W.; Nuzzo, R. G. *J. Phys. Chem. B* **2001**, *105*, 12689.

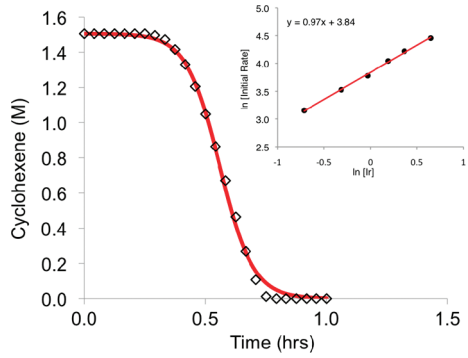

Figure 5. Observed kinetics for the formation of $Ir(0)_{\sim 900}/\gamma\text{-}Al_2O_3$ starting from the Ir(1,5-COD)Cl/γ-Al_2O_3 precatalyst. The diamonds are the experimental data (the error bars are smaller than the symbols), and the red line is the fit to the two-step mechanism. The inset is a ln/ln plot of the slope after the induction period (which correlates with k_2)[18] and as a function of the supported [Ir], a plot done solely as a check to confirm the first-order kinetics in the amount of Ir(1,5-COD)Cl in the Ir(1,5-COD)Cl/γ-Al_2O_3 precatalyst for the k_2 growth step of the two-step mechanism.

fold that of the literature $Ir(0)_n/Al_2O_3$ catalysts examined under the same conditions in our laboratories.[44b]

The high activity of the low-temperature, solution-prepared, coordinatively unsaturated $Ir(0)_{\sim 900}/\gamma\text{-}Al_2O_3$ catalyst is actually as expected, our plan being that a highly active catalyst would result since only *weakly coordinating solvent and the desired reactants* are present in the "*weakly ligated/labile-ligand*" nanoclusters[41,42] [i.e., where acetone solvent, H_2, cyclohexane, and the γ-Al_2O_3 support were the only possible nanoparticle ligands available other than the (nonligand) H^+Cl^-]. We have been working on "weakly ligated/labile-ligand" nanoclusters for some time[41a] and will detail additional results in a forthcoming publication.[42b] Overall, criterion number (iv) listed previously of a prototype system is satisfied considering that $Ir(0)_{\sim 900}/\gamma\text{-}Al_2O_3$ exhibits both high activity, >8200 turnovers/h, and a long lifetime, ≥220 000 total turnovers.

$Ir(0)_{\sim 900}/\gamma\text{-}Al_2O_3$ Catalyst Formation Kinetics in Contact with Solution: Rapid and Real-Time Monitoring of the Supported-Nanoparticle Formation via the Cyclohexene Reporter Reaction Method. Using the cyclohexene reporter reaction[18−22] shown in Scheme 1, we have been able to obtain, easily and quickly, very precise kinetic data for the formation of $Ir(0)_{\sim 900}/\gamma\text{-}Al_2O_3$ and starting from the Ir(1,5-COD)Cl/γ-Al_2O_3 precatalyst (10 kinetic runs, each with up to 60 data points at ±0.025% psig precision out of 40 psig). Also performed and shown in the Supporting Information are (a) the necessary controls for the (lack of a) stirring-rate-dependence (Figure S3), ensuring that no H_2 gas-to-solution mass-transfer limitation effects are present, and (b) a control demonstrating a $[cyclohexene]^0$ dependence (Figure S4). These controls help ensure that the rapid, precise, and extremely useful—but indirect—cyclohexene reporter reaction is actually monitoring the desired $Ir(0)_{\sim 900}/\gamma\text{-}Al_2O_3$ formation kinetics detailed in Scheme 1 (i.e., that the cyclohexene reduction reporter reaction is indeed fast relative to the slower k_1 and k_2 nanoparticle formation steps, Scheme 1, vide supra, and therefore performing properly).

The observed sigmoidal kinetics for the formation of $Ir(0)_{\sim 900}/\gamma\text{-}Al_2O_3$ are shown in Figure 5. The data are nicely fit (R^2 = 0.998(1)) by the two-step mechanism for nanoparticle formation, A → B and A + B → 2B, where A is the Ir(1,5-COD)Cl/γ-Al_2O_3 precursor complex and B is the growing $Ir(0)_n$ nanoparticle surface shown in Scheme 1. The fit shown is obtained from a nonlinear least-squares fit to the analytic integrated rate equation derived from the two-step mechanism;[18] the rate equation and the associated integrated rate equation from the two-step mechanism are provided in the Supporting Information. The resultant fit yields the average rate constants and associated error[69] for nucleation ($k_1 = 1.5(1.1) \times 10^{-3}$ h^{-1}) and autocatalytic surface growth ($k_{2corr} = 1.6(2) \times 10^4$ h^{-1} M^{-1}), where the error bars shown are the experimental error bars (not just the less useful curve-fit errors) derived from 10 independent kinetic runs (including runs from three separately synthesized precatalyst batches and two bottles of commercially available acetone, the latter since nanoparticle formation kinetics have been shown to be sensitive to water and trace impurities in solvents such as acetone).[44b] The reproducibility of the kinetics is generally excellent in comparison to that of the well-studied $Ir(0)_n$ nanoparticle formation system in acetone solution[18,24,69]—once again exhibiting the value of being able to compare the supported to the solution nanoparticle system. The reported k_{2corr} values have been corrected (as mathematically required) for the ∼1700 stoichiometry factor[18] introduced by the cyclohexene reporter reaction, Scheme 3 (the interested reader is referred to the Supporting Information for details regarding this required correction factor). The essential point here is that the resultant $k_{2corr} = k_2$ as defined in Scheme 3.

Further confirmation of the two-step mechanism was obtained by checking the initial rate dependence of the induction period (which correlates primarily with k_1)[18] and the slope after the induction period (which correlates with k_2)[18] of the supported-nanoparticle formation reaction as a function of the Ir(1,5-COD)Cl loading in the Ir(1,5-COD)Cl/γ-Al_2O_3 precatalyst. The Ir wt % loading was varied from 1.0 to 3.85 wt %, corresponding to 0.5−1.9 mM Ir in contact with solution. Consistent with the first-order A → B nucleation step of the two-step mechanism, a ln/ln plot of the nucleation rate (i.e., extracted when ≥0.05 psig of H_2 had been consumed)[18] vs the initial Ir(1,5-COD)Cl/γ-Al_2O_3 precatalyst concentration is linear with a slope of 1.0, within experimental error (Figure S8, Supporting Information). Also, a ln/ln plot of the initial nanoparticle growth rate vs the initial Ir(1,5-COD)Cl/γ-Al_2O_3 precatalyst concentration, shown in the inset of Figure 5, is linear and reveals a slope of 1.0, within experimental error. This further confirms that the autocatalytic growth step (A + B → 2B) of the reaction is first-order in the Ir(1,5-COD)Cl/γ-Al_2O_3 precatalyst (i.e., $[A]^1$) over the concentration range studied.

Overall, the observed kinetics are fully consistent with and strongly supportive of the two-step mechanism of slow continuous nucleation A → B (rate constant, k_1), followed by fast autocatalytic surface growth A + B → 2B (rate constant, k_2) as the *minimum, Ockham's razor mechanism* able to account for the observed kinetic data. Also significant here is that the $Ir(0)_{\sim 900}/\gamma\text{-}Al_2O_3$ supported-nanoparticle formation kinetics (i) are quite reproducible and (ii) result in the formation of a supported, near-monodisperse (i.e., ±≤15%[63]) 2.9 ± 0.4 nm (i.e., ±14%) nanoparticle catalyst. These results mirror the similar good reproducibility and near-monodisperse nanoparticle

(68) Edlund, D. J. Ph.D. Dissertation, University of Oregon, September 1987.

(69) For details on the observed error limits in k_1 of $\pm 10^{1.2}$ h^{-1} and in k_2 of ±3-fold (M^{-1} h^{-1}) derived over a >7 year period from data obtained from multiple investigators, all for the best-studied $P_2W_{15}Nb_3O_{62}^{9-}$ polyoxoanion-stabilized $Ir(0)_{\sim 300}$ nanoparticle system, see: Widegren, J. A.; Bennett, M. A.; Finke, R. G. *J. Am. Chem. Soc.* **2003**, *125*, 10301 (specifically p 10304).

formation kinetics observed for the kinetically and mechanistically well-studied,[18,19,45−47] solution-based $Ir(0)_{\sim 300}$ and $Ir(0)_{\sim 900}$ nanocluster formation systems[69]—the desired, but not previously demonstrated, reproducibility. Therefore, criteria v (real-time monitoring of the nanoparticle formation kinetics) and vi (observed reproducibility of those kinetics and the resultant products) of a prototype system as defined herein are also satisfied, especially with the additional controls checking and verifying the kinetic results obtained via the cyclohexene reporter reaction as described next.

Control of Directly Monitoring the $Ir(0)_{\sim 900}/\gamma$-Al_2O_3 Catalyst Formation Kinetics via Its Cyclooctane Evolution. The choice of Ir(1,5-COD)Cl/γ-Al_2O_3 as a prototype precatalyst in the present work allows for an additional, valuable kinetic monitoring method. Specifically, using GLC, we have directly monitored the cyclooctane evolution kinetics for the conversion of Ir(1,5-COD)Cl/γ-Al_2O_3 to $Ir(0)_{\sim 900}/\gamma$-Al_2O_3 (Figure S7, Supporting Information). The data were fit to the mathematically correct form of the two-step analytic equation derived in the Supporting Information (in which the math shows that the ~1700 stoichiometry factor, required for the cyclohexene reporter reaction, is not required for the GLC kinetics).[70] A good fit is obtained ($R^2 = 0.988$), considering the relatively few and imprecise data points obtainable by the GLC sampling method. The resultant rate constants were obtained, $k_{1GLC} = 1.2(2) \times 10^{-3}$ h^{-1} and $k_{2GLC} = 1.2(2) \times 10^4$ h^{-1} M^{-1}.[71] Quantitatively, the nucleation (k_1) and autocatalytic growth (k_2) rate constants from the GLC cyclooctane evolution kinetics are in good agreement, within experimental error, vs those obtained from the cyclohexene reporter reaction method ($k_1 = 1.5(1.1) \times 10^{-3}$ h^{-1} and $k_{2corr} = 1.6(2) \times 10^4$ h^{-1} M^{-1}), results which provide independent verification of the kinetics of supported-nanoparticle formation. The relatively few, less precise, and much more laboriously obtained GLC kinetic data make apparent the ease, precision, and power of the reporter reaction method developed earlier[18−22] for solution nanoparticle formation, but now applied to heterogeneous catalyst formation in contact with solution. These data further satisfying criterion vi of a prototype system. They also show the value of starting from the well-defined Ir(1,5-COD)Cl/γ-Al_2O_3 precatalyst, a system modeled after the kinetically and mechanistically well-studied solution-based nanoparticle formation system starting from the polyoxoanion-supported organometallic complex, $[Ir(1,5\text{-}COD)\cdot P_2W_{15}Nb_3O_{62}]^{8-}$.

$[Ir(1,5\text{-}COD)Cl]_2$ Kinetics without γ-Al_2O_3 Present: Revealing the Role of the γ-Al_2O_3 Support. The reduction of $[Ir(1,5\text{-}COD)Cl]_2$ in acetone and under 40 psig of H_2 (i.e., identical to the "standard conditions"), *but without γ-Al_2O_3 present*, yields bulk $Ir(0)_n$ metal (Figure 6). Although not unexpected, the results demonstrate that the γ-Al_2O_3 support is crucial for limiting nanoparticle aggregation, and thereby stopping bulk $Ir(0)_n$ formation. Hence, another nice feature of the Ir(1,5-COD)Cl/γ-Al_2O_3 system is its ability to reveal the expected, but virtually undemonstrated,[4] role of the γ-Al_2O_3 support in the nanoparticle formation reactions in contact with solution.

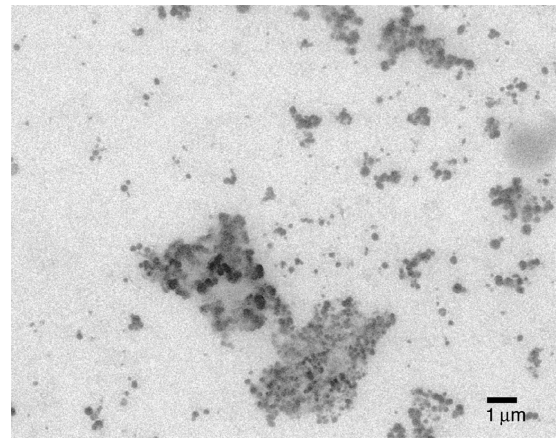

Figure 6. SEM imaging of the observed bulk metal products from the reduction of $[Ir(1,5\text{-}COD)Cl]_2$ in acetone, at 40 psig of H_2 and with stirring at 600 rpm, but *with no γ-Al_2O_3 present*. Note the much larger, now 1 μm (1000 nm) scale bars in comparison to the 5−100 nm scales in the earlier microscopy figures herein.

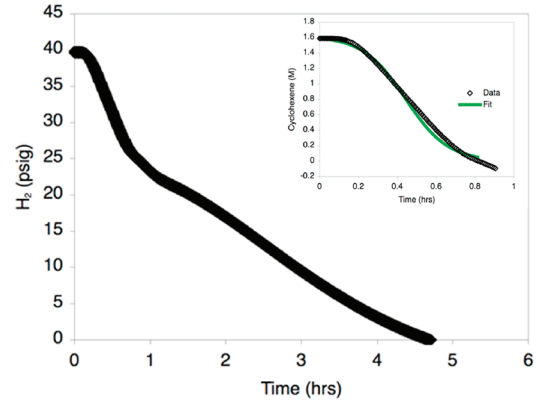

Figure 7. Reduction kinetics from $[Ir(1,5\text{-}COD)Cl]_2$ in acetone, at 40 psig of H_2 and with stirring at 600 rpm (the error bars on the data are smaller than the points shown). The inset is an attempted fit of the early portion of the data to the two-step mechanism of nanoparticle formation, which reveals that the two-step mechanism only partially accounts for most, but not all, of the observed early kinetic data.

Note also that the $[Ir(1,5\text{-}COD)Cl]_2$ reduction kinetics for the formation of bulk $Ir(0)_n$ shown in Figure 7 are significantly different than the $Ir(0)_{\sim 900}/\gamma$-Al_2O_3 supported-nanoparticle formation kinetics (Figure 5, vide supra). Without the γ-Al_2O_3 support, a short induction period is observed, followed by a fast uptake of H_2. Subsequently, an additional, large uptake of H_2 is observed (~1−5 h), corresponding to the hydrogenation of acetone to 2-propanol,[41a] a feature *not* seen in the γ-Al_2O_3-supported $Ir(0)_{\sim 900}/\gamma$-Al_2O_3 catalyst results (vide supra). Since HCl is crucial for the acid-assisted hydrogenation of acetone (added Proton Sponge totally stopping that catalysis, for example),[41a] the suppression of acetone hydrogenation in the γ-Al_2O_3-supported $Ir(0)_{\sim 900}/\gamma$-Al_2O_3 catalyst case is probably the result of alumina buffering[72] the effective pH, thereby inhibiting the otherwise extant HCl-assisted acetone hydrogenation.[41a]

(70) Morris, A. M.; Watzky, M. A.; Agar, J. N.; Finke, R. G. *Biochemistry* **2008**, *47*, 2413.

(71) The reported k_{1GLC} and $k_{2GLCcorr}$ error bars for the GLC data are derived from the non-linear-least-squares fit to the two-step mechanism; that is, they do not correspond to the *experimental error* inherent (i.e., are *fit* errors) to the nucleation and autocatalytic surface growth kinetics obtained from multiple kinetic runs (i.e., and as was obtained for the reported reporter reaction kinetics, $k_1 = 1.5(1.1) \times 10^{-3}$ h^{-1} (i.e., $\sim \pm 10^1$) and $k_{2corr} = 1.6(2) \times 10^4$ h^{-1} M^{-1}).

(72) Buffering effects of γ-Al_2O_3 are known, see for example: Park, J.; Regalbuto, J. R. *J. Colloid Interface Sci.* **1995**, *175*, 239.

When the initial portion of the kinetic data for the reduction of $[Ir(1,5\text{-COD})Cl]_2$ was fit to the two-step mechanism (inset in Figure 7), a statistically worse fit resulted ($R^2 = 0.992$) and the resultant rate constants are $k_1 = 1.4(2) \times 10^{-1}$ h^{-1} and $k_{2corr} = 9.6(5) \times 10^3$ h^{-1} M^{-1} (averages from three separate kinetic runs). Comparing the above rate constants to those obtained from the $Ir(0)_{\sim 900}/\gamma\text{-}Al_2O_3$ supported-nanoparticle formation reaction ($k_1 = 1.5(1.1) \times 10^{-3}$ h^{-1} and $k_{2corr} = 1.6(2) \times 10^4$ h^{-1} M^{-1}) *reveals that the presence of the γ-Al_2O_3 affects primarily the nucleation step and rate constant (k_1)*. Preliminary evidence suggests that the underlying mechanism of this interesting and important effect of the γ-Al_2O_3 support is actually primarily due to the γ-Al_2O_3 operating indirectly by binding relatively tightly, but not completely, the Ir(1,5-COD)Cl—that is, by indirectly controlling the amount of Ir(1,5-COD)Cl *released into solution* where, our current evidence strongly suggests,[74] the actual nanoparticle formation reaction is primarily taking place. While a separate detailed paper has been required to flush out the details of where and how the catalyst formation occurs (i.e., in solution, on the solid support, or both?),[74] both the presence of the solid support and the little-investigated method of nanoparticle catalyst formation *in contact with solution* are important aspects of the present system.

Summary

In conclusion, the following are the primary components and findings of this work:

(i) We presented, and then pursued, the hypothesis that the synthesis, and parallel study of the kinetics and mechanism, of supported-nanoparticle catalysts formed from speciation-controlled, supported organometallics *in contact with solution* is an important way to both (a) prepare a next generation of supported-nanoparticle catalysts with composition, size, and shape control and to (b) help bring what has been developed in the modern "nanoparticle revolution" to supported heterogeneous catalysts and their catalysis.

(ii) We defined eight criteria (vide supra and vide infra) for a so-called prototype system to focus the needed studies.

(iii) We then prepared and characterized the starting material and the product, established the balanced nanoparticle formation reaction stoichiometry, and studied the kinetics of formation of $Ir(1,5\text{-COD})Cl/\gamma\text{-}Al_2O_3$ to $Ir(0)_{\sim 900}/\gamma\text{-}Al_2O_3$, offered as a prototype system for the formation of supported nanoparticles in contact with solution.

(iv) We showed that the kinetics of the nanoparticle formation reaction could be successfully monitored in real time by the cyclohexene reporter reaction method, by GLC as a control, and we also performed controls demonstrating $[cyclohexene]^0$ and stirring-rate-independencies to provide added confidence in the kinetic method(s) and resultant data.

(v) We found that the kinetic data were reproducible and were well-fit by the two-step mechanism of slow, continuous nucleation ($A \rightarrow B$; rate constant $k_1 = 1.5(1.1) \times 10^{-3}$ h^{-1}) and fast, autocatalytic surface growth ($A + B \rightarrow 2B$; rate constant $k_2 = 1.6(2) \times 10^4$ h^{-1} M^{-1}).[18] This is in turn significant in that it means that the nine synthetic and mechanistic insights from the two-step mechanism[73] should, at least in principle, be applicable to the synthesis of supported-nanoparticle heterogeneous catalysts in contact with solution. Moreover, since independent evidence from other groups via XAFS,[23c,d] SAXS,[23e] HRTEM,[23a] and other methods is now appearing for the two-step mechanism [and its four-step extension that includes two agglomeration steps, bimolecular agglomeration $B + B \rightarrow C$ (rate constant k_3) and novel autocatalytic agglomeration $B + C \rightarrow 1.5C$ (rate constant k_4)], this adds further confidence in and support for the broader applicability of the two (and four)-step mechanism(s) of particle formation and agglomeration.

(vi) Overall, we were able to demonstrate that seven of the eight criteria of a "prototype system" defined herein are met by the $Ir(1,5\text{-COD})Cl/\gamma\text{-}Al_2O_3$ to $Ir(0)_{\sim 900}/\gamma\text{-}Al_2O_3$ system. Specifically, the offered system met the criteria of a prototype system: (i) where a compositionally and structurally well-defined supported precatalyst was developed and employed; (ii) where the system was in contact with solution and a lower temperature reaction (at least to start) was employed with the goal of minimizing further speciation of the precatalyst;[6,36] (iii) where one both could and did establish the balanced stoichiometry of the supported-nanoparticle formation reaction en route to also well-defined supported-nanoparticle products; (iv) where an active and long-lived catalyst resulted (in the present case TOF 2.2−4.8 higher than literature $Ir(0)_n/Al_2O_3$ catalysts and ≥220 000 total turnovers, both for the test reaction of cyclohexene hydrogenation); (v) where a rapid, quantitative, real-time kinetic monitoring method was applied to the forming supported-nanoparticle heterogeneous catalyst; and (vi) where reproducible kinetic data were obtained so that reliable, quantitative conclusions could be drawn [$k_1 = 1.5(1.1) \times 10^{-3}$ h^{-1}; $k_2 = 1.6(2) \times 10^4$ h^{-1} M^{-1}].

Developing systems such as the $Ir(1,5\text{-COD})Cl/\gamma\text{-}Al_2O_3$ to $Ir(0)_{\sim 900}/\gamma\text{-}Al_2O_3$ supported-nanoparticle system herein open up the pursuit of criterion viii, namely a systematic variation of key synthetic variables en route to ideally superior supported-nanoparticle catalysts with especially improved composition control, but also in principle rational size and shape control. Important here is the demonstration that the nanoparticle

(73) Finney, E. E.; Finke, R. G. *Chem. Mater.* **2009**, *21*, 4692. The cited work lists nine insights from the two-step mechanism—insights that are also expected to apply at least in general to the present $Ir(0)_{\sim 900}/\gamma\text{-}Al_2O_3$ supported catalyst system formed in contact with solution (and given (a) the excellent fits of the sigmoidal kinetics to the two-step mechanism and (b) that the first three insights from the two-step mechanism have been verified by the results presented herein): (i) nearly monodisperse (≤±15%) size distributions typically result from the syntheses where the observed kinetics are sigmoidal;[66] (ii) on average, "magic-number sized" nanoparticles tend to be formed, and (iii) avoiding H_2 gas-to-solution MTL ensures the formation of those near monodisperse products (±∼14% in the present case).[48] Along with these already-observed insights for the present $Ir(0)_{\sim 900}/\gamma\text{-}Al_2O_3$ supported catalyst system, six additional mechanistic insights are therefore expected to apply: (iv) rational size control should be possible via a recent nanoparticle size vs time equation in terms of k_1, k_2, and $[A]_0$;[73] (v) additional size control should be possible via added ligands that can control k_1 and k_2 (some initial results are briefly presented in the Supporting Information herein); (vi) the use of seeded growth methods should allow rational, mechanistically guided synthesis of all possible geometric isomers of multimetallic "nano-onions";[66] (vii) rational catalyst shape control should be possible via ligands capable of attaching to the otherwise autocatayctically growing nanoparticle facets, effectively preventing autocatalytic surface growth at that facet;[73] (viii) nanoparticle surface ligands should be able to provide additional nanoparticle stability if desired[73]—an important area of future investigation; and finally (ix) nanoparticle size-dependent bond energies (i.e., surface metal-to-ligand bond energies) as previously found are expected,[20−22] which can change the nanoparticles' fractional surface coverage and change whether smaller or larger nanoparticles are the superior catalysts in a given reaction.[20−22]

(74) Mondloch, J. E.; Finke, R. G. Heterogeneous Catalyst Formation in Contact with Solution: Kinetic Evidence for Homogeneous, Solution Nucleation and Growth for In Situ Supported-Nanoparticle Formation From the Prototype $Ir(1,5\text{-COD})Cl/\gamma\text{-}Al_2O_3$ to $Ir(0)_{\sim 900}/\gamma\text{-}Al_2O_3$ System (tentative title), manuscript in preparation.

formation appears to happen primarily in solution, off the support—research that has required its own, separate study, the results of which will be reported in due course.[74]

Experimental Section

Materials. All solvents and compounds used were stored in a drybox prior to use. Acetone (water content <0.5%) was purchased from Burdick & Jackson and packed under nitrogen. Anhydrous ethyl acetate (Aldrich, 99.8%), anhydrous cyclohexane (Aldrich, 99.5%), decane (Aldrich, ≥99%), propylene carbonate (Aldrich, 99.7%), $[Ir(1,5\text{-COD})Cl]_2$ (STREM, 99%), $[Ir(1,5\text{-COD})\mu\text{-}OCH_3]_2$ (STREM, 98%), and $Ir(CO)_2(acac)$ (STREM, 98%) were all used as received. Cyclohexene (Aldrich, 99%) was freshly distilled over Na metal, under argon, and then stored in a drybox. Acidic activated γ-Al_2O_3 (Aldrich) with a surface area of 155 m^2/g was dried at 160 °C in air for 24 h. Nanopure 18 MΩ-cm H_2O was used from an in-house purification system. H_2 gas purchased from General Air (>99.5% purity) was passed through O_2- and H_2O-scavenging traps (Trigon Technologies) before use.

Analytical Instrumentation and Procedures. Unless otherwise reported, all reaction solutions were prepared under O_2- and moisture-free conditions in a Vacuum Atmospheres N_2-filled drybox. The O_2 level (always ≤5 ppm; typically ≤1 ppm) was continuously monitored by a Vacuum Atmospheres O_2 sensor. IR spectroscopy was run on a Nicolet 380 FT-IR instrument in transmission mode, and the data were analyzed using OMNIC software; 256 scans were collected for each spectrum at a resolution of 4 cm^{-1}. XAFS experiments were performed at beamline X-19A at the National Synchrotron Light Source (NSLS, Brookhaven National Laboratory, Upton, NY). The storage ring energy was 2.5 GeV, and the ring current was in the range of 110−300 mA. A double-crystal Si(111) monochromator was used to scan the X-ray energy from 150 to 1400 eV relative to the Ir L_3-edge (11 215 eV). Gas−liquid chromatography (GLC) was performed using a Hewlett-Packard 5890 Series II chromatograph, along with a flame-ionization detector and equipped with a Supelco SPB-1 (Aldrich, 30 m × 0.25 mm ×0.25 μm) fused silica column. The GLC parameters were as follows: initial oven temperature, 50 °C; initial time, 3.0 min; rate, 10 °C/min; final temperature, 160 °C; injector temperature, 180 °C; detector temperature, 200 °C; and injection volume, 2 μL. TEM analysis was conducted at Clemson University with the expert assistance of JoAn Hudson and her staff. ICP-OES analysis for the detection of Ir on the $Ir(1,5\text{-COD})Cl/\gamma\text{-}Al_2O_3$ precatalyst was done at Galbraith Laboratories.

Precatalyst Preparation: $Ir(1,5\text{-COD})Cl/\gamma\text{-}Al_2O_3$. All of the precatalysts were prepared in a drybox using preselected $[Ir(1,5\text{-COD})Cl]_2$ to γ-Al_2O_3 weight-to-weight ratios. For example, a 2.0% weight-to-weight $Ir(1,5\text{-COD})Cl/\gamma\text{-}Al_2O_3$ sample was prepared by the following procedure by adding 1.0 g of acidic γ-Al_2O_3 to 20 mg of $[Ir(1,5\text{-COD})Cl]_2$ (in 15 mL of ethyl acetate), corresponding to a 2.0 wt % sample (i.e., wt % = [wt$[Ir(1,5\text{-COD})Cl]_2$/(wt$[Ir(1,5\text{-COD})Cl]_2$ + wt γ-Al_2O_3) × 100, as this is what we measure experimentally and hence know). Specifically, the appropriate amount of $[Ir(1,5\text{-COD})Cl]_2$ was weighed in a 20 mL scintillation vial. A new 5/8 in. × 5/16 in. Teflon-coated octagon-shaped stir bar was added to the vial, and the solid was dissolved in 15 mL of ethyl acetate. The appropriate amount of solid oxide (e.g., 1.0 g of acidic γ-Al_2O_3 for the 2.0 wt % Ir catalyst) was added by pouring the metal-oxide into the vial (i.e., this order of addition is deliberate, and the indicated equilibration time is important, vide infra), and the solution was stirred for 24 h to equilibrate the $[Ir(1,5\text{-COD})Cl]_2$ with the solid oxide and the solution. After 24 h, the reaction was taken to dryness in a drybox by placing the sample under vacuum for 8 h at room temperature. A control reaction using the opposite order of addition (i.e., in which the γ-Al_2O_3 was stirred in the ethyl acetate solution and the $[Ir(1,5\text{-COD})Cl]_2$ was added to that stirring solid) yielded a darker grayish-yellow solid. The resultant catalyst formation kinetics were still sigmoidal; however, a ∼0.2 h induction period was observed (vs 0.5(1) h for the reverse order of addition), yet the quantitative k_1 and k_{2corr} rate constants were within experimental error of the "standard conditions" preparation. The resulting supported precatalysts were stored in a drybox.

Carbon Monoxide IR Spectroscopy Experiments. To start, 300 mg of the 2.0 wt % $Ir(1,5\text{-COD})Cl/\gamma\text{-}Al_2O_3$ precatalyst was placed in 5 mL of cyclohexane in a drybox. The solution was transferred into a culture tube (containing a 5/8 in. × 5/16 in. Teflon-coated stir bar), sealed inside the FP bottle, and attached to a gas line containing CO. The CO was admitted into the FP bottle at 20 psig, and the reaction vessel was purged every 30 s until 2.5 min had passed (i.e., for a total of five purges), all while stirring the solution at 300 rpm. After 10 min, the FP was vented, resealed, and transferred back into the drybox. The solution was dried under vacuum for 4 h, yielding a beige solid. A KBr pellet was pressed (in a drybox) out of a physical mixture of KBr and the beige solid and transferred under N_2 outside the drybox to the IR instrument (i.e., in a jar sealed under N_2), and its IR spectrum was recorded.

The authentic $Ir^I(CO)_2/\gamma\text{-}Al_2O_3$ sample was prepared by slurrying 20 mg of $Ir(CO)_2(acac)$ in ethyl acetate with 1.0 g of γ-Al_2O_3 in a manner identical to the $Ir(1,5\text{-COD})Cl/\gamma\text{-}Al_2O_3$ precatalyst synthesis described above.

XAFS Sample Preparation and Measurements. XAFS experiments were performed at beamline X-19A at the NSLS. The samples were prepared in a glovebox under N_2 by brushing a fine powder uniformly onto an adhesive tape, which was then folded several times to achieve a suitable total thickness for the measurement. Measurements were carried out in a sealed cell purged with high-purity He. Specifically, Ir L_3-edge (edge energy = 11 215 eV) EXAFS spectra (taken from 150 below to 1400 eV above the Ir_3 edge energy) were obtained for the $Ir(1,5\text{-COD})Cl/\gamma\text{-}Al_2O_3$ precatalyst, the reference compounds $[Ir(1,5\text{-COD})Cl]_2$ and $[Ir(1,5\text{-COD})\mu\text{-}OCH_3]_2$, and the supported-nanoparticle product $Ir(0)_{\sim 900}/\gamma\text{-}Al_2O_3$. Ir(0) black was measured in reference mode simultaneously for the X-ray energy calibration and data alignment. Ion chambers with suitable gas mixtures were employed to record the intensity of the incident, transmitted, and reference beams in transmission mode. The γ-Al_2O_3-supported samples are low (∼2%) in Ir content; therefore, fluorescence data collection was utilized. The fluorescence signal was measured using a Lytle detector filled with Ar gas. Zn filter and Soller slits were used to minimize scattering.

XAFS Data Analysis. Data processing and analysis were performed using the IFEFFIT package. EXAFS analysis was done by fitting the theoretical functions calculated with FEFF6 to the experimental data in *r*-space. All the fitted data were limited to the first nearest neighbor (1NN) contributions. The passive electron factors, S_0^2, were found to be 0.80 by fits to the Ir(0) black standard and then fixed for further analysis of the $Ir(0)_n/\gamma\text{-}Al_2O_3$ supported nanoparticles. The parameters describing the electronic properties (e.g., correction to the photoelectron energy origin) and local structure environment (coordination numbers *N*, bond lengths *R*, and their mean-squared disorder parameters σ^2) around the absorbing atoms were allowed to vary during fitting. The $Ir(1,5\text{-COD})Cl/\gamma\text{-}Al_2O_3$ precatalyst and the reference compound $[Ir(1,5\text{-COD})Cl]_2$, due to their molecular, nonmetallic nature, have significant differences in electronic structure compared to metallic Ir. Therefore, we separately obtained $S_0^2 = 1$ from the fit to the reference compound $[Ir(1,5\text{-COD})\mu\text{-}OCH_3]_2$ while constraining $N_{Ir-C} = 4$ and $N_{Ir-O} = 2$ based on its known structure, and then fixed $S_0^2 = 1$ in the fits of the precatalyst as well as the $[Ir(1,5\text{-COD})Cl]_2$ model compound. The photoelectron path between Ir and its carbon nearest neighbors (Ir−C) was used to simulate both the Ir−C and Ir−O contributions, as C and O are not readily distinguishable by EXAFS analysis. Additionally, a physically reasonable constraint, setting the CN(Ir−C) + CN(Ir−Cl) = 6, was applied in the EXAFS data fits for the precatalyst as well as $[Ir(1,5\text{-COD})Cl]_2$. The XANES $Ir(1,5\text{-COD})Cl/\gamma\text{-}Al_2O_3$ precatalyst spectrum was analyzed by fitting via a linear combination of spectra from the reference compounds $[Ir(1,5\text{-COD})Cl]_2$ and $[Ir(1,5\text{-COD})\mu\text{-}OCH_3]_2$ to approximate the substitution of chloride by oxo ligands from the γ-Al_2O_3 support,

which could not be clearly demonstrated from the EXAFS analysis. Specifically, the XANES spectra for the Ir(1,5-COD)Cl/γ-Al_2O_3 precatalyst compound as well as both references were properly aligned and normalized. Subsequently, the spectra in the energy range of -5 to 18 eV relative to the Ir L_3 absorption edge were subjected to linear combination fitting, whereby the sum of weighting factors of the two reference spectra was constrained to be equal to 1.

Hydrogenation Apparatus and Data Handling. Hydrogenation experiments for monitoring the H_2 reduction of Ir(1,5-COD)Cl/γ-Al_2O_3 to Ir(0)$_n$/γ-Al_{23} were carried out in a previously described apparatus[18−22,44,46,48,49] to continuously monitor H_2 pressure loss. Briefly, the apparatus consisted of a FP bottle modified with Swagelock TFE-sealed Quick-Connects to both a H_2 line and an Omega PX621 pressure transducer. The pressure transducer is interfaced to a PC through an Omega D1131 5 V A/D converter with a RS-232 connection. Reactions were run at a constant temperature by immersing the FP bottle in a 500 mL jacketed reaction flask containing dimethyl silicon fluid (Thomas Scientific), which was regulated by a thermostatted recirculating water bath (VWR). Pressure uptake data were collected using LabView 7.1. The hydrogen uptake curves were converted to cyclohexene (M) curves using the previously established 1:1 H_2/cyclohexene stoichiometry.[18,44] The data were also corrected for the acetone solvent vapor pressure using the previously established protocol.[49] Specifically, either one can measure the acetone vapor pressure independently and subtract that curve (point-by-point) from the raw H_2 uptake data during the cyclohexene reporter reaction, or one can simply back-extrapolate the experimental vapor pressure rise (seen in the induction period of the reaction).[49] Both methods yield the same k_1 and k_2 rate constants within $\pm$15%. The cyclooctane formation and cyclohexene kinetic curves were fit to the analytic equations (equations S4 and S5, respectively, in the Supporting Information) for nucleation and autocatalytic surface growth of nanoparticle formation, A $\rightarrow$ B, rate constant k_1, plus A + B $\rightarrow$ 2B, rate constant k_2 (see Scheme 2),[70] using nonlinear least-squares fitting in Origin 7.0.[49]

Formation of the Active Catalyst: Standard Conditions Reaction. In a drybox, 0.05 g of the Ir(1,5-COD)Cl/γ-Al_2O_3 catalyst precursor was weighed into a 2 dram vial and transferred to a culture tube. To ensure a quantitative transfer, 2.5 mL of acetone and 0.5 mL of cyclohexene were added to the 2 dram vial. The solution was then transferred via a disposable polyethylene pipet into a new borosilicate culture tube (22 $\times$ 175 mm) with a new 5/8 in. $\times$ 5/16 in. Teflon-coated octagon-shaped stir bar. The culture tube was sealed in the FP bottle, removed from the drybox, and attached to the H_2 line. The sealed, H_2-line-attached FP bottle was placed into a temperature-regulated water bath set at 22.0 $\pm$ 0.1 °C. A standard conditions purge cycle[18,44] was used to initiate the reaction, a series of H_2-flushing cycles in which the FP bottle was purged with H_2 every 15 s until 3.5 min had passed (a total of 14 purges). The stir plate was started and set at 600 rpm to allow the H_2 gas-to-solution equilibrium, and the H_2 pressure was then set to 40 psig, with the data recording started 4 min after the purge cycle began (i.e., by definition $t = 0$ for the kinetics).

Confirmation of the Molecularity ([A]^1) for Autocatalytic Surface Growth, A + B $\rightarrow$ 2B. A series of precatalysts from 1.0 to 3.85 wt % were made as described above ("Pre-Catalyst Preparation: Ir(1,5-COD)Cl/γ-Al_2O_3"). In each case, the maximum rate after the induction period was obtained through a linear least-squares fit in Excel.

GLC Cyclooctane Evolution Kinetics and Determination of the Ir(1,5-COD)Cl/γ-Al_2O_3 Reaction Stoichiometry. The procedure employed was very similar to that previously published.[48] In a drybox, 0.05 g of the Ir(1,5-COD)Cl/γ-Al_2O_3 catalyst precursor was weighed into a 2 dram vial. The Ir(1,5-COD)Cl/γ-Al_2O_3 precatalyst was transferred into a new borosilicate culture tube (22 $\times$ 175 mm) with a new 5/8 in. $\times$ 5/16 in. Teflon-coated octagon-shaped stir bar. To ensure a quantitative transfer, 1.5 mL of acetone, 1.0 mL of a 0.292 mM decane/acetone solution (used as an internal standard), and 0.5 mL of cyclohexene were added to the 2 dram vial. The solution was then transferred via a disposable polyethylene pipet into the culture tube containing the Ir(1,5-COD)Cl/γ-Al_2O_3 precatalyst. A "standard conditions" hydrogenation was started (vide supra). At predetermined times, the stirring was stopped, the H_2 pressure was released from the FP bottle (but keeping a positive H_2 pressure of $\geq$15 psig), and aliquots ($\leq$0.1 mL) of the reaction solution were drawn with a 9 in. needle attached to a gastight syringe. After the aliquot was drawn, the FP bottle was resealed, stirring was restarted at 600 rpm, and the FP was purged five times (once every 5 s) and then allowed to fill to 40 psig (30 s). Before each aliquot was drawn, the needle was rinsed with acetone 10 times and then thoroughly dried with compressed air.

H_2 Uptake Experiments. A 1.0 g sample of the 2.0 wt % Ir(1,5-COD)Cl/γ-Al_2O_3 precatalyst was placed in 7.5 mL of propylene carbonate in a culture tube in a drybox. The reaction was run following the "standard conditions" protocol, except the solution was stirred at 1000 rpm.

[Ir(1,5-COD)Cl]$_2$ Reduction Kinetics without γ-Al_2O_3 Present. A 0.98 mg (0.974 mM) sample of [Ir(1,5-COD)Cl]$_2$ was weighed into a 2 dram vial. Next, 2.5 mL of acetone and 0.5 mL of cyclohexene were added to the 2 dram vial via gastight syringe. The resultant yellow solution was mixed with a polyethylene pipet and transferred into a new borosilicate culture tube (22 $\times$ 175 mm) with a new 5/8 in. $\times$ 5/16 in. Teflon-coated octagon-shaped stir bar. The reaction was continued following the same procedure as in the "Standard Conditions Reaction" section.

Cyclohexene Turnover Frequency Experiments: Calculations and Assumptions. The TOF was determined using a preformed Ir(0)$_{\sim 900}$/γ-Al_2O_3 catalyst, generated as described in the "Formation of the Active Catalyst: Standard Conditions Reaction" section above. After 1.5 h (i.e., after 1 equiv of cyclooctane per Ir is known to be evolved), the FP bottle was brought back into the drybox. The FP bottle was opened, and an additional 3.0 mL of cyclohexene was added to the reaction solution. The FP was sealed, brought back out of the drybox, and placed on the hydrogenation line, where another "standard conditions" purge cycle was performed, and stirring resumed at 600 rpms. Over the course of 4 h, the reaction took up on average 69.36 psig of H_2, an average between two independent experiments. The TOF was calculated from a calculated dispersion (D = surface atoms/total atoms), assuming that all the Ir(0)$_{\sim 900}$/γ-Al_2O_3 surface atoms were active.[75] The total (average) number of Ir atoms was estimated from the TEM data by the formula $N = \pi D_f^3 \rho N_A/6MW$.[44] Applying this formula, one obtains on average Ir(0)$_{\sim 900}$ nanoparticles. Using the magic-number approximation,[66] there are on average 362 Ir atoms present at the surface of each Ir(0)$_{\sim 900}$ nanoparticle, yielding a dispersion of 39%. This calculation assumes that the Ir(0)$_{\sim 900}$ nanoparticles observed by TEM are spherical, a reasonable approximation to their true shape.[76]

Total Turnover Demonstration. The Ir(0)$_{\sim 900}$/γ-Al_2O_3 catalyst was prepared as described in the "Standard Conditions" section. After 1.5 h (i.e., when 1 equiv of cyclooctane per Ir had evolved), the FP bottle was brought back into the drybox. The solution was transferred into a 20 mL scintillation vial and dried overnight. Next, 0.01 g of the catalyst material was weighed out into a 20 mL

(75) (a) More rigorously, "the number of exposed metal atoms determined by chemisorption experiments in the solid state is not necessarily equivalent to the number of catalytically active surface sites in solution", see p 1626 and footnote 10 in Hornstein, B. J.; Aiken, J. D., III; Finke, R. G. *Inorg. Chem.* **2002**, *41*, 1625. Other references of relevance: (b) Gonzalez-Tejuca, L.; Namba, A. S.; Turkevich, J. *J. Phys. Chem.* **1977**, *81*, 1399. (c) Kivrak, H.; Mastalir, A.; Kiraly, Z.; Uner, D. *Catal. Commun.* **2009**, *10*, 1002.

(76) Supported nanoparticles can take on many different morphologies; for a few examples, see: (a) Henry, C. R. *Prog. Surf. Sci.* **2005**, *80*, 92. (b) Pakarinen, O. H.; Barth, C.; Foster, A. S.; Henry, C. R. *J. Appl. Phys.* **2008**, *103*, 054313. (c) Haruta, M. *CATTECH* **2002**, *6*, 102.

scintillation vial, then 5.0 mL of cyclohexene was added (corresponding to a maximum of 85 000 TTOs per total Ir and 220 000 TTOs per surface Ir atom), and the solution was transferred via a polyethylene pipet into a new borosilicate culture tube (22 × 175 mm) with a new 5/8 in. × 5/16 in. Teflon-coated octagon-shaped stir bar. The standard conditions purge cycle was used, stirring was set at 600 rpm for 3.5 min, and the solution was left open to 40 psig of H_2. After 86 h, GLC confirmed 100% conversion of cyclohexene to cyclohexane with no observable undesirable side products. We note here that the use of the $Ir(0)_{\sim 900}/\gamma$-Al_2O_3 catalyst under these specific conditions (i.e., with only cyclohexene and cyclohexane present as solvent) led to the catalyst sticking to the borosilicate culture tube, thereby considerably slowing the reaction.

Preparation of TEM Grids. Following a "standard conditions" supported-nanoparticle formation reaction, and 0.5 h after the complete hydrogenation (i. e., after 1.0 equiv of cyclooctane per Ir had evolved), the FP bottle was transferred into the drybox. A 300 mesh Formvar-coated SiO_2 TEM grid was dipped in the sample for approximately 5 s and then allowed to dry. The grid was placed in a 2-dram vial, wax-sealed, placed in a 20 mL scintillation vial, and sent for TEM analysis.

Acknowledgment. R.G.F. and J.E.M. gratefully acknowledge support from the Chemical Sciences, Geosciences and Biosciences Division, Office of Basic Energy Sciences, Office of Science, U.S. Department of Energy, grant SE-FG02-03ER15453. The authors thank Dr. JoAn Hudson for expert assistance with the TEM imaging. A.I.F. and Q.W. acknowledge support from the U.S. Department of Energy, grant DE-FG02-03ER15476. Use of NSLS was supported by the U.S. Department of Energy, Office of Science, Office of Basic Energy Sciences, under Contract No. DE-AC02-98CH10886. Beamline X19A at the NSLS is supported in part by the Synchrotron Catalysis Consortium, U.S. Department of Energy Grant No DE-FG02-05ER15688.

Supporting Information Available: EXAFS 1NN fitting results for the Ir(1,5-COD)Cl/γ-Al_2O_3, $Ir(0)_{\sim 900}/\gamma$-Al_2O_3 catalyst, as well as the $[Ir(1,5\text{-COD})Cl]_2$ and $[Ir(1,5\text{-COD})\mu\text{-}OCH_3]_2$ model compounds; additional TEM images along with particle size histograms for the $Ir(0)_{\sim 900}/\gamma$-Al_2O_3 catalyst, as well as controls for mass-transfer limitations and plots demonstrating a zero-order cyclohexene dependence; the two-step rate law and integrated rate equation as well as the k_2 correction factor for the ~1700 cyclohexene stoichiometry factor; cyclooctane evolution kinetics from the 2.0 wt % Ir(1,5-COD)Cl/γ-Al_2O_3 catalyst; TEM imaging and cyclooctane evolution kinetics when cyclohexene is absent from the synthesis. This material is available free of charge via the Internet at http://pubs.acs.org.

JA1030062